Collective dynamics in a model of sliding charge-density waves. I. Critical behavior

Christopher R. Myers* and James P. Sethna
Laboratory of Atomic and Solid State Physics, Cornell University, Ithaca, New York 14853-2501
(Received 25 June 1992; revised manuscript received 19 January 1993)

The dynamics and critical phenomena of the depinning transition in charge-density-wave (CDW) systems are explored, primarily through simulations of an automaton model that we have developed to characterize the essential features of the standard Fukuyama-Lee-Rice (FLR) treatment of CDW's. We first provide an overview of the dynamics of the class of FLR models, and then derive our automaton model. We report results of simulations above and below the depinning transition, focusing primarily on the behavior of the CDW velocity above threshold and the growth of dynamic correlations on both sides of the transition. The critical exponent ζ describing the scaling of the CDW velocity is estimated in $d=1$, 2, and 3, in agreement with estimates of ζ from simulations of related CDW models and a recent renormalization-group calculation. The velocity-velocity correlation above and below the transition is described in terms of "avalanches" between different configurations. A companion paper examines the unusual finite-size effects evident in the sliding state.

I. INTRODUCTION

Charge-density-wave (CDW) conductors exhibit a rich response to applied electric fields which involves many dynamical degrees of freedom. This complicated dynamics arises from the competition between the random pinning of the CDW by impurities and/or defects and the elasticity of the CDW itself. One important consequence of this competition is the existence of a depinning transition which involves collective CDW dynamics on long length scales. Within a certain class of models, the process of depinning can be interpreted as a phase transition between the pinned and sliding states of the CDW.[1] A diverging dynamical correlation length can be identified near the transition, and power-law scaling is observed in the manner of traditional equilibrium phase transitions.

A detailed understanding of the dynamics and critical phenomena associated with the depinning transition has been rather slow in developing, however. Much of the insight into the critical phenomena has come through numerical simulations,[2–6] although an earlier mean-field analysis[1] and a recent renormalization-group (RG) calculation[7] have also contributed substantially. Numerical studies of the critical phenomena of sliding CDW's have been hampered, however, by unusually small critical regions and the existence of slow time scales near threshold. As a result, it is only recently—through the numerical work presented here, in conjunction with numerical[4] and analytic[7] work by others—that a consensus seems to have been reached with regard to the numerical values of the basic scaling exponents characterizing the transition.

One reason for continued interest in sliding CDW's has been a major focus on the dynamics and criticality of other driven, nonlinear, many-degree-of-freedom systems, such as models of sandpiles[8–10] and earthquakes.[11] Many such systems display a rich spatiotemporal response to external driving. In particular, many spatially extended, driven systems exhibit a broad distribution of dynamical event sizes,[8] and unusual finite-size scaling properties have also been noted.[9,10] CDW's exhibit distributions of event sizes and unusual finite-size scaling properties, although the CDW does not strictly exhibit "self-organized criticality"[8] as is found in other systems, since the criticality of depinning is the result of the fine tuning of an external parameter. It is nonetheless useful to interpret, when possible, the behavior of CDW's in terms of this larger class of systems.

It is our goal to elucidate certain aspects of the dynamics and critical phenomena of CDW's in an applied dc field. This will be done primarily within the context of a model we have developed which incorporates the essential features of the Fukuyama-Lee-Rice (FLR) model of CDW's. To conclude Sec. I, we outline the scaling theory of the depinning transition and present the standard lattice implementation of the FLR model. In Sec. II, we provide an overview of the dynamics of the lattice FLR model, and then derive and construct an automaton model which is based on this model. Our automaton model is both practical, as it speeds considerably simulations of CDW's near threshold by circumventing the slow motions which characterize the system, and insightful, as it emphasizes those aspects of the dynamics which appear to be relevant to the critical phenomena, namely, the rapid hopping of unstable phases and the subsequent destabilization of neighboring phases. In Sec. III, we present results of simulations of this automaton model to estimate various critical exponents describing the CDW both above and below threshold. In particular, we compute the CDW velocity exponent ζ and correlation length exponent ν in the sliding state. The velocity exponent ζ (in $d=1$, 2, and 3), as measured in our automaton model, agrees within errors with that estimated by Middleton[4] in simulations of a variety of other continuous-phase and discrete-phase models as well as with that calculated in $4-\epsilon$ dimensions by Narayan and Fisher.[7] In examining the relevant correlation length—in this case, the velocity-velocity correlation length ξ—we introduce a graphical representation which conveys the nature of the

dynamic correlation and which suggests anomalous finite-size effects in the sliding state. We discuss these finite-size effects in more detail in a companion paper which immediately follows this paper. We also define and measure a dynamic correlation length and its scaling below threshold, by considering a characteristic avalanche size connecting stable fixed points in the pinned state.

A. Depinning as a critical phenomenon

The existence of a (fairly) sharp transition between the pinned and sliding states in CDW conductors[12] invites the interpretation of the depinning transition as a type of critical phenomenon.[1] We highlight this scaling theory here. The depinning transition is driven by the application of an external dc field F, with the transition occurring at a threshold field F_T. We define a reduced driving field $f \equiv (F - F_T)/F_T$, where F_T is the threshold field for a *particular* sample (particular size, dimensionality, impurity configuration, pinning strengths, etc.). The order parameter for the depinning transition is the average steady-state CDW velocity v, which is expected to scale, in the thermodynamic limit, as a power-law in f for $f \gtrsim 0$:

$$v \sim f^{\zeta} . \tag{1}$$

This implies a diverging time scale $T \equiv 1/v$, such that $T \sim f^{-\zeta}$, where T is the time required for the periodic CDW orbit to repeat itself. Furthermore, there is expected to be a diverging length scale, which is, in this theory, the velocity-velocity correlation length ξ. The scaling exponents ν and ν' describe the divergence of this length scale above and below the transition, respectively:

$$\xi \sim f^{-\nu} \quad (f > 0) , \tag{2}$$

$$\xi \sim f^{-\nu'} \quad (f < 0) . \tag{3}$$

B. Lattice FLR model

A standard lattice version of the Fukuyama-Lee-Rice[13] model has been developed[14] and studied[15] by several authors. The lattice FLR model describes the dynamics of the CDW phase $\phi_i(t)$ at each site i on a d-dimensional (hyper)cubic lattice with periodic boundary conditions. The disorder of impurity pinning is implemented via a quenched random pinning phase β_i at each lattice site. The Hamiltonian is this lattice model describes the effects of an applied electric field, the CDW elasticity, and pinning by disorder:

$$H = -F \sum_i \phi_i + \tfrac{1}{2} J \sum_{\langle ij \rangle} (\phi_i - \phi_j)^2 - \frac{V}{2\pi} \sum_i \cos[2\pi(\phi_i - \beta_i)] , \tag{4}$$

where F is proportional to the applied electric field, V is the strength of the pinning potential, J is the elastic coupling strength (with appropriate scaling to make the elastic constants isotropic), and the β_i are drawn uniformly from the interval [0,1). Because the CDW's motion is highly overdamped, the CDW inertia is typically neglected, and ϕ_i evolves according to relaxational dynamics:

$$\dot{\phi}_i = -\frac{\delta H}{\delta \phi_i} = F + J\Delta_i^2(\phi) - V \sin[2\pi(\phi_i - \beta_i)] , \tag{5}$$

where

$$\Delta_i^2(\phi) = \sum_{\langle j \rangle} (\phi_j - \phi_i) \tag{6}$$

is the finite-difference curvature (lattice Laplacian) of the phase field ϕ at site i, the sum being over nearest neighbors $\langle j \rangle$ to site i. This model treats the CDW as an array of overdamped, zero-temperature, harmonically coupled,[16] randomly pinned oscillators subject to a spatially uniform driving field. The pinning strength V is also sometimes chosen to fluctuate randomly from site to site, but it is believed this does not alter the universality of the critical behavior.[2] This model is typically simulated in the strong-pinning limit ($V \gg J$) so that individual phases ϕ_i correspond more or less to phase-coherent Lee-Rice domains in the CDW.[2]

II. DYNAMICS OF THE CDW

In this section we provide an overview of the dynamics of driven, deformable CDW's, emphasizing those elements which are central to the derivation of our simplified automaton model. We begin by considering the dynamics of a single degree of freedom, and then present a weak-coupling analysis of the full system, en route to deriving the automaton.

A. Dynamics of a single degree of freedom

The decoupling of neighboring phases in the lattice FLR model (5) yields the following equation of motion for each phase ϕ_i on the lattice:

$$\dot{\phi}_i = F - V \sin[2\pi(\phi_i - \beta_i)] . \tag{7}$$

This equation has fixed-point solutions ($\dot{\phi}_i = 0$) only for $F \leq V$. For larger fields, the phase ϕ slides indefinitely. The depinning transition at $F = V$ is a saddle node bifurcation, which we depict schematically in Fig. 1; we plot

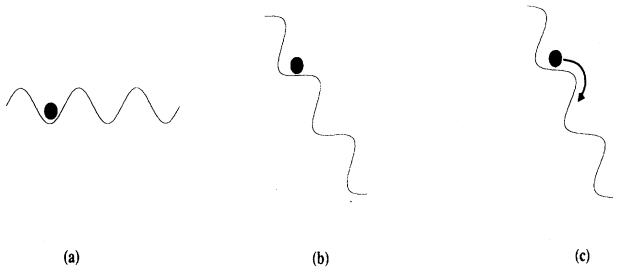

FIG. 1. Schematic dynamics in the single-coordinate model, for (a) $F = 0$, (b) $F = V$, and (c) $F > V$. For $F \leq V$, there is a fixed point, where the local potential surface is flat, but for $F > V$ there is no such fixed point, and the CDW hops from one potential well to the next. This hopping leads to the motion shown in Fig. 2.

the position and velocity of the single phase ϕ in Fig. 2.

The sliding motion of the phase is periodic, repeating itself in a time T, which depends upon the excess driving field $F-V$. Just above threshold, the motion is dominated by a sticking point. This is the remnant of the fixed point which existed below threshold, and is associated with motion through a region of the potential surface which is almost flat, as is depicted in Fig. 1(c). Near threshold, almost the entire period T is consumed by the traversal of this sticking point, but most of the phase increment associated with sliding occurs during a rapid jump which follows the escape from the sticking point. The sliding behavior of the single-coordinate model can be solved for completely by integrating the equation of motion (7):

$$\phi_i(t)=\beta_i+n_i(t)+\tfrac{1}{4}+\frac{1}{\pi}\tan^{-1}\left[\frac{1}{\sqrt{F-V}}\tan(\pi\sqrt{F^2-V^2}\,t)\right], \quad (8)$$

where $n_i\equiv\text{nint}(\phi_i-\beta_i-\frac{1}{4})$, nint$(x)$ being the nearest integer to x. The period T of the motion is the time required for the phase ϕ_i to increment by 1:

$$T=\int_{\phi_i}^{\phi_i+1}\frac{d\phi_i'}{F-V\sin[2\pi(\phi_i'-\beta_i)]}=\frac{1}{\sqrt{F^2-V^2}}, \quad (9)$$

which implies $v\equiv 1/T=\sqrt{F^2-V^2}$. For small f, therefore, $v\sim f^{1/2}$. The interpolation between square-root scaling at small reduced fields and linear scalings at large f can be seen in Fig. 3, where we plot the "local velocity exponent" $\zeta_{\text{loc}}\equiv d(\log_{10}v)/d(\log_{10}f)$.

B. Dynamics of the lattice FLR model

Once many randomly pinned phases are coupled together, there are many distinct coexisting fixed points below threshold, in contrast with only one in the single degree-of-freedom case. (Like the single-degree-of-freedom case, however, the transition itself is unique and nonhysteretic, and the sliding state above threshold is unique and periodic for models satisfying "no passing," as described by Middleton.[17]) The sliding state in the many-degree-of-freedom system is dominated by the spectrum of sticking points which arise from the bifurcations of the many fixed points below threshold. We show this in Fig. 4, where the spatially averaged velocity in a small system is seen to wax and wane as various phases hop rapidly and slow in their motion through sticking points.

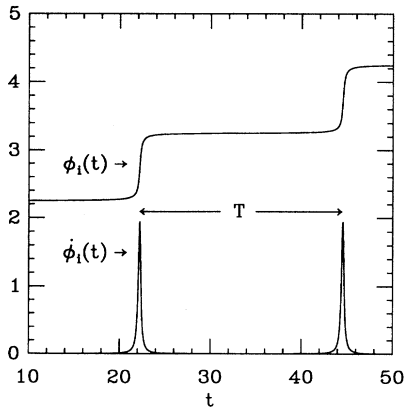

FIG. 2. Phase trajectory $\phi_i(t)$ and phase velocity $\dot{\phi}_i(t)$ for a single phase [Eq. (7)], with $F=1.001$, $V=1.0$, and $\beta_i=0$. The jerky motion exhibited here is an important feature of the sliding CDW.

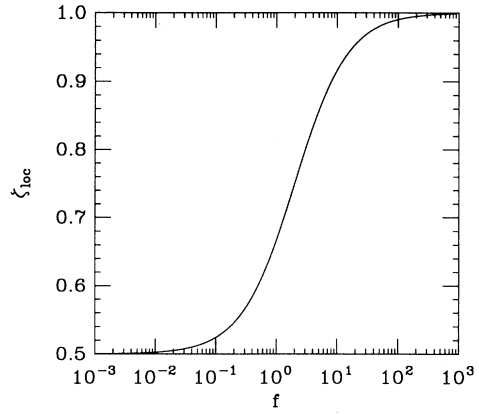

FIG. 3. The local velocity exponent $\zeta_{\text{loc}}\equiv d(\log_{10}v)/d(\log_{10}f)$ for a single-coordinate CDW. The velocity interpolates between a square-root scaling form ($\zeta_{\text{loc}}=0.5$) at small f and linear scaling ($\zeta_{\text{loc}}=1.0$) at large f.

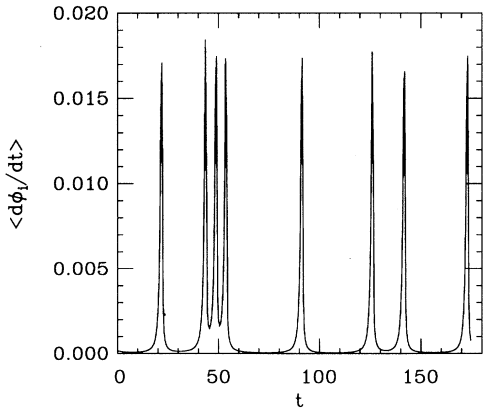

FIG. 4. The time evolution of the spatially averaged velocity $\langle\dot{\phi}(t)\rangle$ in the sliding state, for a one-dimensional system of size 8^1, demonstrating the role of sticking points (velocity minima) and phase hoppings (velocity maxima). Compare this with Fig. 12 of Ref. 6, an analogous plot for the Frenkel-Kontorova model, where pinning is incommensurate rather than random. The uneven spacing between phase hops and the unequal minimum velocities in the CDW arises from the disorder inherent in the pinning.

1. *Weak-coupling limit*

Because of the existence of many sticking points, the dynamics of the lattice FLR model are slow to simulate; the motions are also difficult to characterize. As a result, we were led to consider its dynamics in the limit of weak coupling, $J \ll V$, both to speed simulations and simplify the motion of the system.[18] We begin by plotting in Fig. 5 each of the local phase velocities for a small one-dimensional system ($L=8$), to illustrate how instability propagates through the system. This figure demonstrates that (1) phase motions are triggered by the hops of neighboring phases, and (2) unstable phases can spend considerable time moving slowly through sticking points after being destabilized.

We seek solutions to the equations

$$\dot{\phi}_i = F + J\Delta_i^2(\phi) - V\sin[2\pi(\phi_i - \beta_i)] \tag{10}$$

for all sites i on the lattice, in the limit $J \ll V$. We expand the ϕ_i about the $J=0$ threshold configuration,

$$\phi_i \equiv \beta_i + \tfrac{1}{4} + n_i + \delta_i \ , \tag{11}$$

where $n_i \equiv \text{nint}(\phi_i - \beta_i - \frac{1}{4})$ and $\delta_i \in [-\frac{1}{2}, +\frac{1}{2})$ represents a local phase deviation. Then (10) becomes

$$\dot{\delta}_i = F + J\Delta_i^2(\beta + \tfrac{1}{4} + n + \delta) - V\cos(2\pi\delta_i) \ . \tag{12}$$

Even though the CDW just above threshold is not static, individual phases (in the weak-coupling limit) spend most of the time moving very slowly, sitting near their threshold fixed points, with all the δ_i near zero. We expand the field F and each of the δ_i in powers of $J^{1/2}$.

$$\delta_i = a_1^i J^{1/2} + a_2^i J + a_3^i J^{3/2} + \cdots \ , \tag{13}$$

$$F = F_T^0 - b_1 J^{1/2} - b_2 J - b_3 J^{3/2} - \cdots \ , \tag{14}$$

and then expand the cosine pinning potential for small argument:

$$[\dot{a}_1^i J^{1/2} + \dot{a}_2^i J + O(J^{3/2})] = F_T^0 - [b_1 J^{1/2} + b_2 J + O(J^{3/2})] - V(1 - \tfrac{1}{2}\{2\pi[a_1^i J^{1/2} + O(J)]\}^2 + O(J^2))$$
$$+ J\{\Delta_i^2(\beta+n) + [\Delta_i^2(a_1)J^{1/2} + \Delta_i^2(a_2)J + O(J^{3/2})]\} \ . \tag{15}$$

We solve $\dot{a}_k^i \equiv 0 \forall i,k$ order by order in $J^{1/2}$. To $O(J^{1/2})$,

$$b_1 = 0 \ , \tag{16}$$

so that the threshold field F_T is not shifted to $O(J^{1/2})$. To $O(J)$,

$$-b_2 + 2\pi^2 V (a_1^i)^2 + \Delta_i^2(\beta+n) = 0 \ , \tag{17}$$

implying

$$a_1^i = -\left[\frac{b_2 - \Delta_i^2(\beta+n)}{2\pi^2 V}\right]^{1/2} \ . \tag{18}$$

(The negative branch of the square root is selected for reasons of stability.) Equation (18) places a constraint on b_2 since all the solutions a_1^i must be real:

$$b_2 \geq \max\{\Delta_i^2(\beta+n)\} \ . \tag{19}$$

Since b_2 describes [to $O(J)$] the shift in the field F, we see that the zeroth-order configuration $\{\beta+n\}$ will find a fixed point (i.e., will have no unstable phases) for fields

$$F \leq F_T^0 - J\max\{\Delta_i^2(\beta+n)\} \ . \tag{20}$$

For a fixed realization $\{\beta\}$, there may be fixed points at larger fields, but these will involve different zeroth-order configurations, i.e., rearrangements of the integer field $\{n\}$.

We can use this criterion to identify those sites which, for a zeroth-order configuration $\{\beta+n\}$, are unstable [to $O(J)$]. We deem a site unstable, or "active," if it satisfies

$$\Delta_i^2(\phi) > C \ , \tag{21}$$

where

$$C \equiv (V - F)/J \ . \tag{22}$$

We have introduced here an "activation curvature" C, the largest curvature that a site can sustain while still being stable.

The fixed-point solutions presented above are not so useful in describing the full sliding dynamics, so we consider the dynamics of $\delta_i(t)$ for the sites which are unstable as defined by Eq. (21). Since the large hopping motions of unstable phases are primarily responsible for the redistribution of phase strain in the system, we wish to predict the time at which an unstable phase will hop forward, after being destabilized. We start with Eq. (12):

$$\dot{\delta}_i = F + J\Delta_i^2(\beta + \tfrac{1}{4} + n + \delta) - V\cos(2\pi\delta_i) \ . \tag{23}$$

The first two terms on the right hand side of this equation make up the local effective driving field $\mathcal{F}_i(t)$. In general, this would have a complicated time dependence. In the weak-coupling limit, however, phases remain very close to the zero-coupling threshold fixed points, $\phi_i \approx \beta_i + \frac{1}{4} + n_i$, for almost the full period T, and deviate from those fixed points only for a short time to hop by a full wavelength. Therefore, we can approximate the space of allowed phase configurations to be the discrete set

$$\phi_i = \beta_i + \tfrac{1}{4} + n_i \ , \tag{24}$$

and the space of allowed motions to be only integer hops,

$$n_i \rightarrow n_i + 1 \ . \tag{25}$$

Having made these approximations, Eq. (23) reduces to

$$\dot{\delta}_i = F + J\Delta_i^2(\beta + \tfrac{1}{4} + n) - V\cos(2\pi\delta_i) \ . \tag{26}$$

It is our intention that the dynamics of the δ_i be fictitious, in that we will not numerically integrate their motions as part of the simulation. Since we are only concerned with the dynamics of δ_i insofar as the fact that a large enough increase in δ_i brings about an integer hop,

$$(\delta_i \rightarrow +\tfrac{1}{2}) \Longrightarrow (n_i \rightarrow n_i + 1) , \tag{27}$$

we wish to analytically integrate the equation of motion of an unstable phase to the point at which it hops.

Having discretized the allowed configurations and allowed motions, we can perform an analytical integration of Eq. (26), since the time dependence of the effective driving field $\mathcal{F}_i(t)$ is no longer arbitrarily complicated.

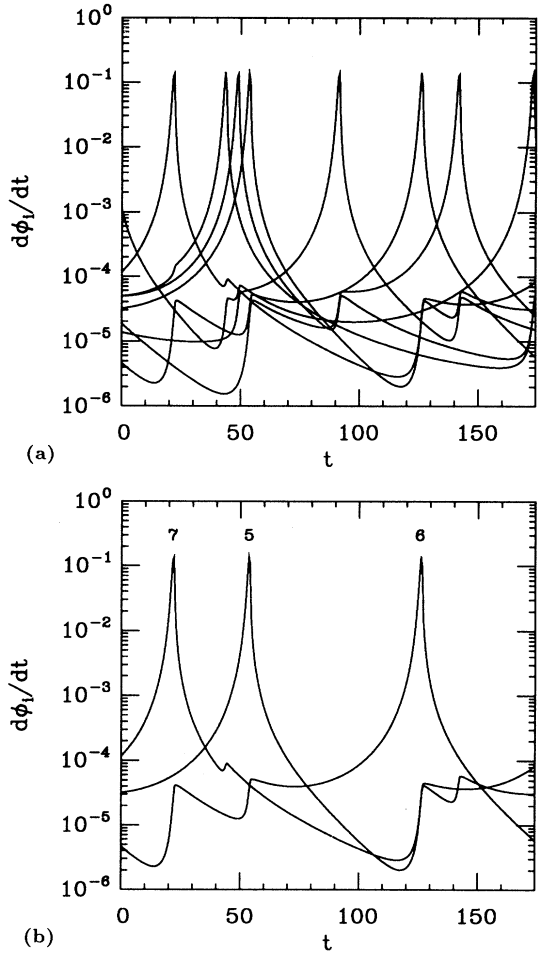

FIG. 5. Dynamics of the lattice FLR model for weak coupling, in a one-dimensional system of size $L=8$. In (a) the local phase velocities $\dot{\phi}_i$ are shown for all eight sites, while in (b) we have plotted only $\dot{\phi}_i$ for $i=5$, 6, and 7, which label the three velocity curves. The simulation is done for $V=1.5$, $J=0.001$, $F=1.5$. In (b) three important processes are evident: (1) the destabilization of a phase by the hopping of a neighbor (e.g., 6 being destabilized by 5 hopping at $t\approx 54$); (2) the slow motion of an unstable phase through a sticking point (e.g., site 6 reaching a velocity minimum at $t\approx 70$); and finally (3) the hopping of an unstable phase (e.g., site 6 at $t\approx 125$).

The coupling term $J\Delta_i^2(\beta+\frac{1}{4}+n)$ is constant in time unless a neighboring site j hops ($n_j \rightarrow n_j+1$) while site i is active. Therefore, *if* the neighboring sites j are stationary (nonhopping) during the time that site i is active (in the process of hopping), Eq. (26) reduces to a single-degree-of-freedom equation of motion. Defining the local weak-coupling curvature c_i as

$$c_i \equiv \Delta_i^2(\beta+n+\tfrac{1}{4}) , \tag{28}$$

we rewrite Eq. (26) as

$$\dot{\delta}_i = \mathcal{F}_i - V\cos(2\pi\delta_i) , \tag{29}$$

where the effective driving field $\mathcal{F}_i \equiv F + Jc_i$ is a piecewise constant function in time, changing by discrete amounts instantaneously when either site i or a neighboring site j hops. With a piecewise constant effective driving field $\mathcal{F}_i$, we can integrate exactly Eq. (29) to find the time evolution of $\delta_i(t)$:

$$t(\delta_i) = \frac{1}{\pi\sqrt{\mathcal{F}_i^2 - V^2}} \tan^{-1}\left[\frac{\tan\pi\delta_i}{\sqrt{\mathcal{F}_i - V}}\right] , \tag{30}$$

$$\delta_i(t) = \frac{1}{\pi}\tan^{-1}\left[\frac{1}{\sqrt{\mathcal{F}_i - V}}\tan(\pi\sqrt{\mathcal{F}_i^2 - V^2}\,t)\right] . \tag{31}$$

These equations are valid only if no neighboring sites j hop between the time when site i is activated and the time when site i hops. If there is such a hopping event, then we must recompute the projected hopping time of site i, which is, of course, possible since the new effective driving field $\mathcal{F}_i$ is constant in time until another neighbor hops.

2. *Global dynamics from local motions*

In the previous section we described how a single unstable phase moves. To piece together these local motions, we appeal to Fig. 5, which provides insight into the time evolution of the coupled dynamical system. Our approach is to develop a scheme whereby we identify which sites are unstable, compute at what time in the future they will hop (using the results of Sec. II B 1), and then accelerate forward to those points in time when phases hop, without having to wade through all times in between when no phases are moving appreciably.

A site is unstable, according to Eq. (21), if $c_i > C$. Barring any changes in the parameters V, F or J, this will happen only if a neighboring phase ϕ_j hops and increases the curvature at site i. As is clear in Fig. 5, once a site is destabilized, it begins to move forward from its initial position at activation, through the sticking point, and finally to the hopping time at which point its velocity is a maximum. (Since most of the phase motion occurs in a very short time around the velocity maximum, we refer to the time of maximum velocity as the hopping time. This approximation should not qualitatively affect the dynamics.) In the weak-coupling limit, the initial position of the unstable phase is given, to lowest order in J, by Eq. (18). This is the distance an unstable phase must travel as it works its way "in" to the sticking point. Once the

phase passes through the velocity minimum, it must work its way "out" of the sticking point, until it finally "hops" at $\delta_i = \frac{1}{2}$. Once it hops, its neighbors may become unstable as well.

3. *The discrete-phase time-lag CDW automaton model*

Having derived various results in the weak-coupling limit and outlined how to piece together the motions of individual hopping phases, we state here the complete set of rules for the operation of our discrete-phase time-lag automaton model.

(1) We construct a d-dimensional hypercubic lattice of linear size L with periodic boundary conditions, and identify individual sites on that lattice with an integer index i.

(2) We specify a quenched random pinning phase β_i for each site i on the lattice, drawing the β_i uniformly from the interval [0,1). (The set $\{\beta\}$, for a specified lattice size L and dimensionality d, define a "sample.")

(3) We define a phase ϕ_i for each site i on the lattice, with ϕ_i given by $\phi_i = \beta_i + \frac{1}{4} + n_i$, for n_i integer. As the β_i are quenched, the only dynamics in the model involves the integer component of the phase, n_i.

(4) For a given phase configuration, we calculate the local curvatures $c_i \equiv \Delta_i^2(\phi) = \Delta_i^2(\beta) + \Delta_i^2(n)$.

(5) We set the parameters V, J, and F, and calculate from them the activation curvature $C \equiv (V - F)/J$.

(6) To begin the dynamics, we initialize the running clock time t to $t = 0$. Then we determine which sites are unstable ("active"), i.e., those sites satisfying $c_i > C$. For those sites with $c_i > C$, we calculate a projected hopping time t_i^*, which is the sum of the current clock time t and the projected time lag τ_i^*:

$$t_i^* = t + \tau_i^* . \tag{32}$$

The projected time lag τ_i^* is composed of two pieces, a time $\tau_i^{\text{in}*}$ to move "in" to the sticking point after activation and a time $\tau_i^{\text{out}*}$ to move "out" of the sticking point to the hopping point (velocity maximum):

$$\tau_i^* = \tau_i^{\text{in}*} + \tau_i^{\text{out}*} . \tag{33}$$

The time lags $\tau_i^{\text{in}*}$ and $\tau_i^{\text{out}*}$ are given by the appropriate integrations of Eq. (29). The time "in" to the sticking point reflects the motion from the initial perturbative deviation δ_i^0, given by [see Eqs. (13) and (18)]

$$\delta_i^0 = -\left[\frac{C - c_i}{2\pi^2 V}\right]^{1/2} J^{1/2} , \tag{34}$$

to the sticking point at $\delta_i = 0$. The time "out" reflects the motion from the sticking point at $\delta_i = 0$ to the hopping point at $\delta_i = \frac{1}{2}$. Therefore, using $t(\delta)$ as specified in Eq. (30),

$$\tau_i^{\text{in}*} = t(\delta_i^0) = \frac{1}{\pi\sqrt{\mathcal{F}_i^2 - V^2}} \tan^{-1}\left[\frac{\tan\pi\delta_i^0}{\sqrt{\mathcal{F}_i - V}}\right] , \tag{35}$$

$$\tau_i^{\text{out}*} = t(\tfrac{1}{2}) = \frac{1}{2\sqrt{\mathcal{F}_i^2 - V^2}} . \tag{36}$$

(7) The dynamics proceeds by identifying the site which is scheduled to hop next, namely, that site (call it site i) with earliest hopping time t_i^*. Then the running clock time t is set to the appropriate hopping time,

$$t = t_i^* , \tag{37}$$

and the phase at site i is incremented by 1:

$$n_i \rightarrow n_i + 1 . \tag{38}$$

In accordance with the definition of the lattice Laplacian, the curvatures of site i and its neighbors $\langle j \rangle$ are altered as

$$c_i \rightarrow c_i - 2d , \tag{39}$$

$$c_j \rightarrow c_j + 1 . \tag{40}$$

(8) The neighboring sites $\langle j \rangle$ are then checked to determine if they are unstable, i.e., if $c_j > C$. If a neighboring site j is unstable, then its projected hopping time is computed. The particular calculation of the hopping time depends on whether or not site j was already active prior to the hopping of site i.

(8a) If the neighboring site j was not active prior to the hopping of site i, then the hopping time t_j^* is computed exactly as described in item (6), given by $t_j^* = t + \tau_j^*$, with τ_j^* given as the sum of Eqs. (35) and (36).

(8b) If the neighboring site j was active prior to the hopping of site i, then its projected hopping time must be recomputed. We calculate how far through the hopping process site j had proceeded prior to the hopping site i, and then compute a new projected hopping time based on its current position and its new curvature. Let Δt_j be the amount of time that has elapsed on the running clock time t since site j was last activated, $(\tau_j^{\text{in}*})'$ the previous projected "in" time for site j, $\mathcal{F}_j$ the effective driving field at site j, and $\mathcal{F}_j'$ the effective driving field at site j prior to the hopping of site i ($\mathcal{F}_j' = \mathcal{F}_j - 1$). We compute from the elapsed time Δt_j the current position δ_j^0 via Eq. (31):

$$\delta_j^0 = \frac{1}{\pi}\tan^{-1}\left[\frac{1}{\sqrt{\mathcal{F}_j' - V}} \tan\{\pi\sqrt{(\mathcal{F}_j')^2 - V^2}[(\tau_j^{\text{in}*})' - \Delta t_j]\}\right] . \tag{41}$$

The current position δ_j^0 plays exactly the same role as the initial position δ_i^0 did in item (6) above. Hence we calculate a new projected hopping time $t_j = t + \tau_j^*$ precisely as in item (6), Eqs. (33), (35), and (36) (with j replacing i in those equations). In this formalism, the new "in" time $\tau_j^{\text{in}*}$ can be negative, if $\Delta t_j > (\tau_j^{\text{in}*})'$. This simply reflects the fact that site j had already passed through the velocity minimum before site i hopped.

(9) Once all active sites are accounted for, we return to steps (7) and (8) to increment the next scheduled hopping site and check its neighbors for activity.

4. Simulations

In this section we outline the manner in which we perform simulations of our automaton model. We generate a "sample" as described in points (1) and (2) in the previous section. Then a pinning strength V and a coupling strength J are specified. Typically, we set $J=1$ and then set V so that the threshold field is roughly unity: $F_T \approx 1$.

Once V and J are set, we need to determine the threshold field F_T for the particular sample at hand. This is typically done by starting from a flat configuration ($\phi_i=\beta_i+\frac{1}{4}$; $n_i=0$), identifying the site with the largest local curvature c_i, setting the field F so as to make that site barely unstable ($F \gtrsim V-\max\{c_i\}J$), iterating the CDW until once again stable, and continuing the process of destabilizing the least stable site until the threshold field and threshold configuration has been reached. We can use the "no passing" rule[4,17] to identify the threshold configuration, since the rule implies that any avalanche involving N hops in which all sites hop only once must be an avalanche in the sliding state rather than in the pinned state.[4]

We define a threshold curvature C_T, the largest local curvature in the threshold configuration. The threshold field, in the weak-coupling limit, depends parametrically on V and J and is a function of the threshold curvature C_T:

$$F_T=V-JC_T \ . \tag{42}$$

Whereas F_T depends upon the particular choice of V and J, the threshold curvature C_T only depends on dimension d and the realization $\{\beta\}$. (For a given dimensionality, there are finite-size fluctuations in C_T which tend to zero as $L \to \infty$.) We find that in $d=1$, $C_T \approx 0.5$ for large L, whereas in all higher dimensions, $C_T \approx (d-1)+0.376$ for large L.[19] Since $J=1$ and we wish $F_T \approx 1$, we choose $V=1.5$ in $d=1$ and $V=d+0.376$ in $d \geq 2$.

To determine the velocity v at a particular field above threshold, we follow the procedures outlined in the previous section and iterate the CDW until a periodic orbit is reached. Because the trajectory in the automaton model is characterized entirely by a sequence of hopping sites and their associated hopping times, we deem an orbit converged when that sequence repeats itself, with the hopping times (modulo the period T) converged to the machine's double precision. The average velocity v is just the inverse of the period T of the orbit, which is immediately accessible. We describe in Sec. III precisely how we measure the velocity-velocity correlation length ξ.

5. The time-lag CDW automaton and the lattice FLR model

Our automaton model appears to be a useful distillation of the dynamics important for the critical behavior of sliding CDW's, emphasizing the large hopping motions of unstable phases rather than the slow motions near sticking points. The automaton is an accurate reproduction of the standard lattice model only in limit of weak coupling, $J \ll V$. Having made the appropriate approximations, however, J/V is formally no longer an independent parameter, since the automaton is always in the weak-coupling limit regardless of the particular values of J and V that we choose. So from the point of view of mimicking the specific dynamical details of the lattice FLR model, we do so only for $J/V \ll 1$.

As far as critical phenomena are concerned, our effort at isolating the important elements of the CDW's motion appears to have been worthwhile since the critical exponents measured in simulations of the automaton agree to within errors with those measured in simulations of the standard lattice FLR model.[5,4,3] This implies that no drastic transition separates our automaton model at weak coupling and the lattice FLR model at larger coupling. Middleton's research into other models with phase hops[4] suggests that the velocity exponent ζ is quite robust in finite dimensions with respect to changes in the exact form of the pinning potential. The renormalization-group analysis of Narayan and Fisher confirms this universality.[7]

There are some computational advantages to the automaton. The analytic integration of the equation of motion for an unstable phase is typically faster than a numerical integration of that equation. Furthermore, the analytic integration does not slow down near threshold. This second feature has enabled us to probe the finite-size regime close to threshold in large systems, which has not been studied in much detail previously. Also, just as we do not have to wade through sticking points above threshold, we do not have to spend long times equilibrating slow, small motions below threshold near critical points as a Lyapunov exponent tends to zero.

Conceptually, the simplifications inherent in the weak-coupling limit—localization of hopping events on particular sites, full (i.e., integer) hopping of sites as they slide, etc.—have been institutionalized in the automaton. This makes it considerably simpler to characterize, describe, and visualize the dynamics: individual hopping sites can be identified; sites are either active or inactive; and a precise active time (amount of time a site remains active before hopping) can be associated with each site.

Our automaton, as embodied in steps (1)–(9) above, is operationally far from "simple," however. Whether or not the time-lag functions need to be included in such detail (i.e., are that many arctangents, tangents, and square roots really necessary?) will be addressed at the end of the paper. We wish to comment here, however, on one feature of our model, which contributes heavily to the computational burden but which seems important to the qualitative behavior of the model.

The concept of "no passing" is an important aspect of the dynamics in the lattice FLR model.[17] (This is the property by which one phase configuration $\boldsymbol{\phi}^{(1)}$ lying entirely "behind" another configuration $\boldsymbol{\phi}^{(2)}$, i.e., $\phi_i^{(1)} \leq \phi_i^{(2)} \forall i$, cannot pass that configuration under the action of the dynamics.) We update the hopping times, as embodied in step (8b) of the model, to ensure "no pass-

ing" in our automaton. This incorporation followed a period of time during the development of the model when step (8b) was not included. In this early version of the model, an active site hopped at its initially projected hopping time regardless of the hopping of neighboring sites. We found that the early model typically did not converge to a periodic orbit. This was especially true at larger fields, when more sites were active and the approximation of ignoring hopping neighbors became poorer. At about this time, we became aware of Middleton's work establishing the relationship between "no passing" and periodicity,[20] and realized the need for our model to satisfy "no passing." Once we included step (8b) to do so, we found that the sliding state converged to a periodic orbit. Our serendipitous observation of failure to converge to a periodic orbit serves to bolster the connections between "no passing," phase slip, and broadband noise (BBN). The automaton without step (8b) violated "no passing" and failed to converge to a periodic orbit, implying some BBN in the noise spectrum.[21]

There are some drawbacks to our model, however. Because we have thrown out all the small motions of phases, we cannot compute from simulations any properties which probe the local environment of phases. Linear polarizabilities (to be distinguished from the nonlinear polarizability which measures the hopping of phases), ac response within local minima, and scaling exponents describing the softening of modes near critical points are all inaccessible from our simulations. To some extent, we believe that these "local" properties are of less interest than the global collective dynamics associated with the hopping of phases.

Aside from limiting our ability to probe the system, however, our neglect of small phase displacements does alter certain aspects of the dynamics of the CDW. The most obvious, and probably the most significant, distortion that our model introduces is a misrepresentation of the threshold state, and, in particular, its uniqueness. In the automaton there is a set of configurations which are stable at the threshold field F_T, where in the lattice FLR model there is only one such state. The reason for the discrepancy is that in the lattice FLR model, small displacements are communicated, however minutely, across the lattice until they destabilize the critical threshold site. Our discrete representation of the allowed configuration space in the automaton is such in that these minute displacements do not necessarily propagate arbitrarily far through the system. Rather, only a subset of avalanches generated throughout the system will engulf the threshold site. We have studied the relationship of a discrete configuration in the automaton model to the associated continuous configuration in the lattice FLR model (i.e., a configuration with the same $\{\beta\}$ and $\{n\}$ but which is allowed to deviate with non-zero $\{\delta\}$). It appears from simulations that those configurations which are stable threshold states in the automaton have analogous configurations in the lattice FLR model with critical points very close to the threshold field, probably within $O(J)$ of F_T. Therefore, our automaton appears not to have introduced a vastly different spectrum of instabilities, but only misrepresents critical points on a scale of $O(J)$. Our misrepresentation of the threshold state appears not to have altered the critical behavior on either side of the transition, but we do not understand at this time all the subtle differences between the discrete-phase and continuous-phase models.

Although the automaton is considerably faster to simulate than the lattice FLR model, it is not without its computational drawbacks. In the process of restructuring the dynamics, we have turned a highly parallel problem into a highly serial one. As a result we cannot take full advantage of advances in parallel computing technology which present perhaps the most natural solution to these types of lattice dynamical systems. Algorithmically, implementation of the automaton requires the ability to sort quickly the newly computed hopping times while also allowing for their quick retrieval. (We store the hopping times in a binary tree.) A further limitation is that the model, as currently implemented, does not conveniently allow for the application of ac fields. This is because a change in the applied field would require not only updating the criterion for local instability but also recomputing the hopping times for those sites that are already active. Unless change in the applied field could be worked into the *analytic* formulation of the problem (that is, the equations determining the hopping times of active sites), the incorporation of ac fields into the simulation would be computationally much more taxing. While an arbitrary time-dependent field may be too cumbersome to incorporate into the model, perhaps not so difficult would be a treatment of pulsed (piecewise constant) fields, such as those used to study pulse memory effects.[22] Nonetheless, we have a model which can be simulated very quickly on relatively small machines, allows us to probe very close to threshold, conceptually simplifies certain aspects of the dynamics, and appears to be in the same universality class as the model from which it was derived.

We have made reference previously to related dynamical systems, such as models of sandpiles.[8–10] Our automaton model is obviously similar in spirit to sandpile automata, and, in fact, was constructed with such automata in mind. The biggest difference between our automaton and all other sandpile-type automata that have been previously studied in the time lag between activation and hopping in our model. In all other automata that we know of, sites which exceed a threshold for instability hop immediately.

III. THE CRITICAL PHENOMENA OF DEPINNING

In this section we describe various aspects of the critical phenomena of the depinning transition, as revealed primarily through simulations of our automaton model. By way of organization, we describe the behavior of the CDW as a function of increasing driving field F. This will enable us to describe the buildup to the threshold state (carried out by a series of larger and larger avalanches), the criticality of the threshold state itself, and finally the depinning and sliding of the CDW (involving the formation of correlated "sliding domains," which are analogous to the avalanches below threshold). We will introduce scaling exponents associated with this cri-

ticality, discuss how we measure them in simulations, and report estimates of their numerical values.

A. Critical dynamics below threshold

The CDW inevitably settles into a fixed point for $F \leq F_T$, such that the steady-state velocity of the CDW is strictly zero within this model. Growing correlations in the motion of the CDW are evident, however, in the transient phase motions between fixed points. These phase rearrangements—or avalanches—are naturally generated as the driving field is ramped up toward the threshold field. More and more fixed points bifurcate with the increasing field until the threshold configuration is reached and the CDW is poised on the edge of stability.

1. Correlation length

We demonstrate the growing correlation length below threshold in Fig. 6, where we show avalanches between fixed points for various values of f. Avalanches are a nonequilibrium, transient response of the system to a perturbation which drives it from a fixed point. Avalanches are typically triggered locally, either by an imposed phase rearrangement (such as that used to generate the avalanches in Fig. 6), or by an increase in the driving field F, which can destabilize one or more phases. To define a correlation length ξ below threshold, we identify a characteristic length from the *distribution* of avalanche sizes $D(s)$. We find (in $d > 1$) that such a distribution exhibits roughly a power-law falloff up to some cutoff size s_{co}, above which the distribution drops rather sharply to zero. We define the correlation length $\xi(f)$ below threshold as the linear size associated with the cutoff in the avalanche distribution. We can generate such a distribution in a variety of ways, but in this study, we have done the following: (1) We first prepare the CDW by (a) fixing the reduced field f to a specific value for $f < 0$, (b) setting the CDW configuration to be initially flat ($n_i = 0 \forall i$), and (c) iterating the CDW until a fixed point is reached; (2) we then generate an avalanche by (a) randomly selecting a site on the lattice, (b) incrementing the phase at that site by 1, and (c) iterating the CDW until once again stable. A distribution of such avalanches is constructed by repeating the avalanche generation [steps (2a)–(2c)], starting each avalanche from the stable state that remains in the aftermath of the previous avalanche. The avalanche size s (total number of hops) and its duration t (total time required for the avalanche do die out) are recorded.

Because of the history dependence of the dynamics for $F < F_T$, there are different ways one might define a correlation length below threshold which probably will give different estimates of the scaling exponent ν'.[23] As de-

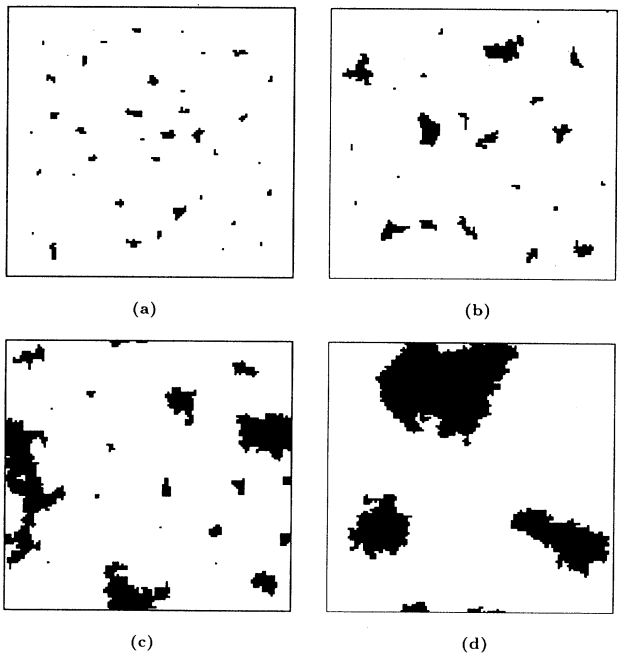

FIG. 6. Avalanches for various $f < 0$ in a system of size 128^2: (a) $f = -0.2$, (b) $f = -0.08$, (c) $f = -0.02$, (d) $f = -0.0065$. Each avalanche (contiguous cluster of shaded sites) is triggered by forcing a single random site to hop forward by one wavelength, and evolving the CDW until once again stabilized. The growth of the correlation length ξ is reflected in the increased avalanche size near threshold.

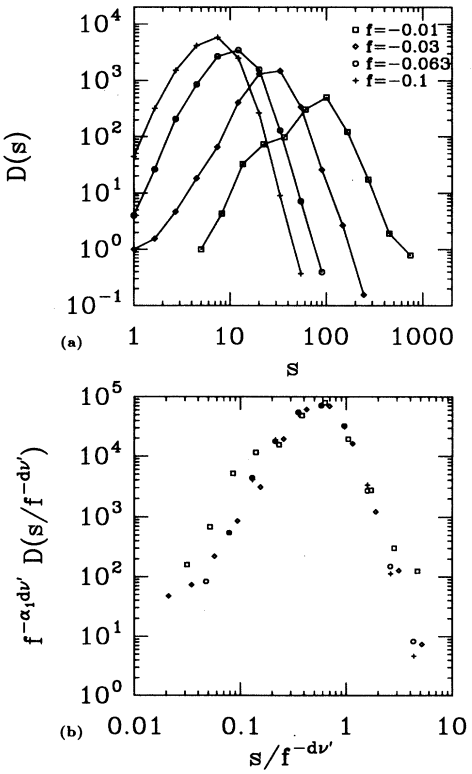

FIG. 7. Avalanche size distribution $D(s)$ for various reduced fields f, in $d = 1$ (a), and associated scaling collapse to extract the correlation length exponent ν' (b). We set $\alpha_s = 1$ for the purposes of this collapse, since it is not well defined in $d = 1$. (See Sec. III B).

scribed above, we generate a distribution of avalanche by driving the system noisily, such that we sample a large extent of the available configuration space. Another approach would be to identify characteristic avalanche sizes triggered by a slow ramping of the applied field F. This method samples a more specific part of the configuration space, namely that accessible on the approach to threshold from a particular initial configuration. The configurations found on approach to threshold are typically less stable[24] than those sampled by a noisy driving at fixed f, and probability more susceptible to finite-size fluctuations.[23] Simulations by Middleton on a related automaton model[25] with avalanches generated by a slow ramping of the driving field apparently yield a correlation length exponent below threshold consistent with an appropriately defined finite-size correlation length exponent, which is larger than the intrinsic exponent ν' we intend to calculate.

We plot in Figs. 7–9 distributions of avalanche sizes $D(s)$ and associated scaling plots to extract the correlation exponent ν', in $d=1$, 2, and 3, respectively. Implicit in the scaling plots is the postulated relationship between the avalanche cutoff size $s_{\rm co}$ and the correlation length ξ.

$$\xi \approx s_{\rm co}^{1/d} \ . \tag{43}$$

Relation (43) is approximate since the avalanche could

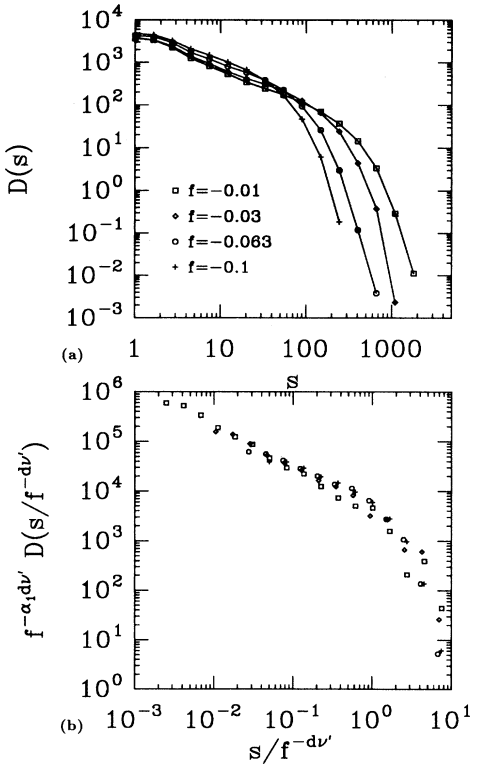

FIG. 8. Avalanche size distribution $D(s)$ for various reduced fields f, in $d=2$ (a), and associated scaling collapse to extract the correlation length exponent ν' (b). The exponent α_s used in the collapse in described in Sec. III B.

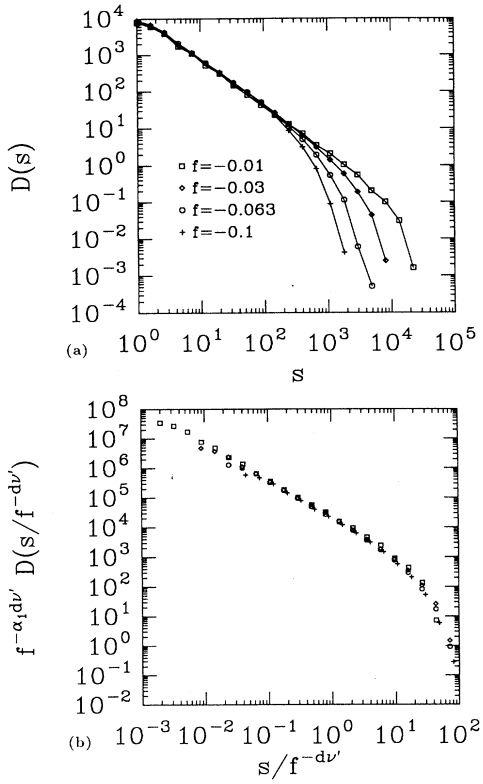

FIG. 9. Avalanche size distribution $D(s)$ for various reduced fields f, in $d=3$ (a), and associated scaling collapses to extract the correlation length exponent ν' (b). The exponent α_s used in the collapse is described in Sec. III B.

have a fractal dimension $D \neq d$. In lieu of actually measuring an avalanche dimension, we approximate it as $D \approx d$, based, in part, on evidence that avalanches in sandpile models have dimensions close to or equal to the underlying spatial dimension.[26,27] (Whether or not the disorder inherent in the CDW will affect these results is unknown). $D(s)$ in $d=1$ is clearly different from that in higher dimensions, in that a power-law falloff for small size s is not apparent. This is related to the "minimal stability" of the CDW in $d=1$. (See Sec. III B for further discussion.) In $d=1$, we associate $s_{\rm co}$ with the peak in the distribution $D(s)$, and in higher dimensions we identify $s_{\rm co}$ from the point where the distribution drops rapidly from the power-law falloff evident for small s.

From the scaling collapses of the distribution functions $D(s)$, we estimate the correlation length exponent below threshold to be

$$\nu' = \begin{cases} 1.1 \pm 0.1, & d=1 \ , \\ 0.6 \pm 0.1, & d=2 \ , \\ 0.45 \pm 0.1, & d=3 \ . \end{cases} \tag{44}$$

We will return later to discuss these results in conjunction with the correlation length exponent ν measured above threshold. The estimated errors account for both the uncertainties in the scaling collapses as well as some

deviation in the fractal dimension D from the underlying spatial dimension.

2. Correlation time

The scaling theory for the depinning transition introduces the exponent ζ to describe the divergence of the time scale T above threshold, but says nothing about the divergence of a macroscopic time scale below threshold. Even though the order parameter v is identically zero below the transition, there is a diverging time scale as revealed by the distribution of avalanche duration times $D(t)$. Because these distributions exhibit a field-dependent cutoff t_{co} at long times in the same manner as the avalanche size distribution is cutoff at s_{co}, we can define a correlation time exponent ζ' which is analogous to the correlation length exponent ν'. In Figs. 10–12, we plot $D(t)$ in $d=1$, 2, and 3, along with scaling collapses to extract ζ'. From the data in these figures, we estimate that

$$\zeta' = \begin{cases} 1.2\pm0.2, & d=1 , \\ 0.55\pm0.15, & d=2 , \\ 0.6\pm0.2, & d=3 . \end{cases} \tag{45}$$

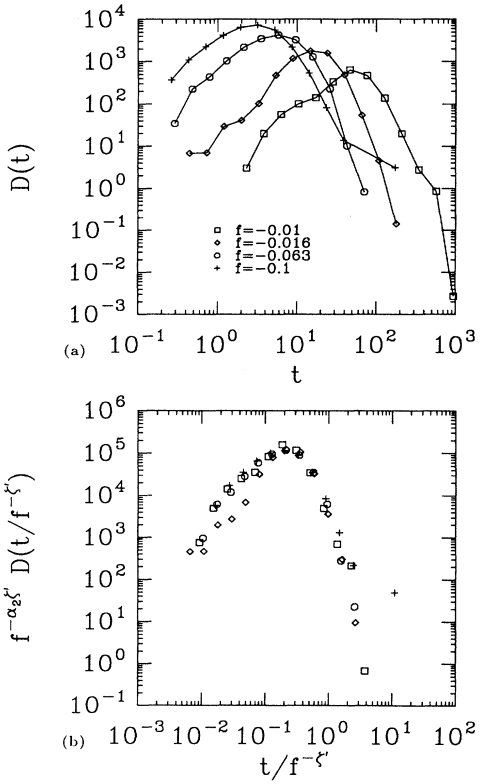

FIG. 10. Avalanche time distribution $D(t)$ for various reduced fields f, in $d=1$ (a), and associated scaling collapse to extract the correlation time exponent ζ' (a). We set $\alpha_t=1$ for the purposes of this collapse, since it is not well defined in $d=1$. (See Sec. III B.)

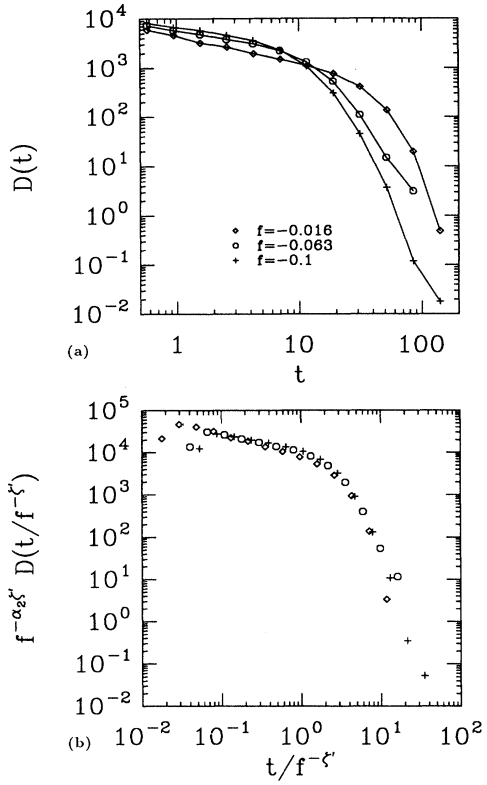

FIG. 11. Avalanche time distribution $D(t)$ for various reduced fields f, in $d=2$ (a), and associated scaling collapse to extract the correlation time exponent ζ' (b). The exponent α_t used in the collapse is described in Sec. III B.

We will comment on these values later, after presenting results above threshold.

3. CDW polarization

Accompanying the growing avalanches near threshold is a growing polarization of the CDW. Whereas the correlation length ξ describes the typical linear size of the CDW response to perturbations, the polarization P describes the total amount of phase transported forward. We define the CDW polarization P with respect to a reference state $\{\hat{\phi}\}$:

$$P=\frac{1}{L^d}\sum_i(\phi_i-\hat{\phi}_i) , \tag{46}$$

where, for definiteness, we set $\{\hat{\phi}\}=\{\beta\}+\frac{1}{4}$. The polarization P is, in our model, simply equal to the total number of hops with respect to the flat configuration.

We are interested in particular in the behavior of the polarization with the driving field f. In the thermodynamic limit, it is expected that the polarization diverges as

$$P\sim|f|^{-\gamma+1} , \tag{47}$$

such that a nonlinear polarizability $\chi^{\uparrow}$ (defined for in-

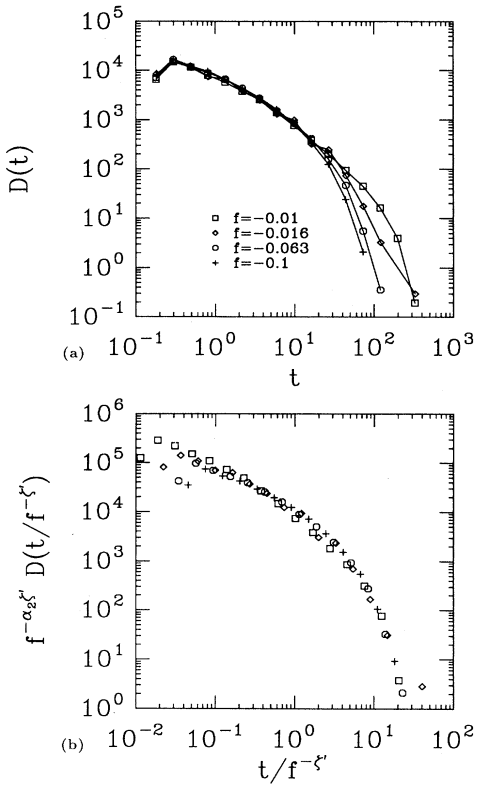

FIG. 12. Avalanche time distribution $D(t)$ for various reduced fields f, in $d=3$ (a), and associated scaling collapse to extract the correlation time exponent ζ' (b). The exponent α_t used in the collapse is described in Sec. III B.

creasing field F) is found to scale as

$$\chi^{\uparrow} \equiv \frac{dP}{df} \sim |f|^{-\gamma} . \tag{48}$$

This nonlinear polarizability is dominated by the large $O(1)$ hops forward rather than the small motions of phases in their local minima. One can also define a linear polarizability[5,4] arising from the small phase motions which precede and follow hops. We will not examine the linear polarizability here.

We present data for $P(|f|)$ which were obtained by starting in the flat configuration $\{\hat{\phi}\}$, increasing the driving field F just enough so as to destabilize a single site, iterating the resulting avalanche to completion, and repeating this process until the threshold configuration is reached. We show, in Figs. 13–15, polarization data in $d=1,2$ and 3, respectively. From the data in these figures, we estimate that

$$\gamma = \begin{cases} 2.8\pm0.1, & d=1 , \\ 1.7\pm0.1, & d=2 , \\ 1.6\pm0.2, & d=3 . \end{cases} \tag{49}$$

The result in $d=2$ agrees with that reported by Middleton[4] for the lattice FLR model. It is inconsistent with his result for $d=1$, although we were able to simulate a larger system than he was.

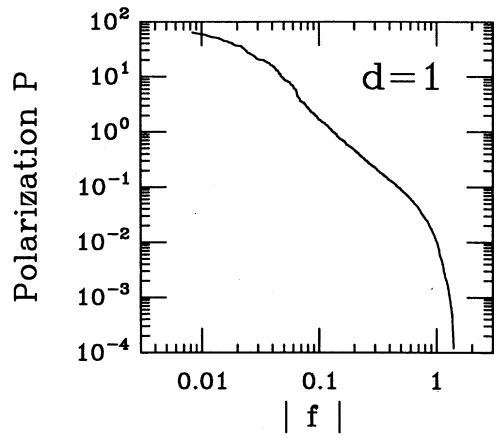

FIG. 13. Polarization of the CDW in $d=1$, for a system of size 8192^1.

B. Threshold state in the automaton model

As the field F is increased to the threshold field F_T, the CDW builds up to the threshold state, teetering on the brink of instability. In this section, we describe certain aspects of this threshold state.

As was described in Sec. II, a major difference between the automaton model and the lattice FLR model is the lack of uniqueness of the threshold configuration. While there is one and only one state in the lattice FLR model which is stable at $F=F_T$, there is a set of such states in the automaton, since small strains are not transmitted arbitrarily far across the system. For this reason, much of what we say regarding the threshold configuration will be particular to the automaton.

Like some sandpile models[8] which it resembles, the automaton model builds up to a qualitatively different configuration at threshold in $d=1$ than it does in all higher dimensions. This difference is one of "minimal"

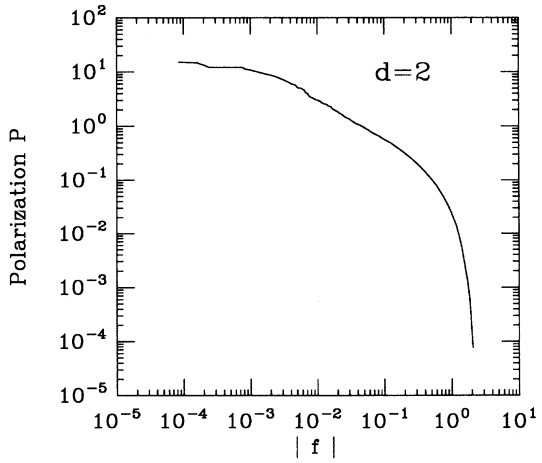

FIG. 14. Polarization of the CDW in $d=2$, for a system of size 256^2.

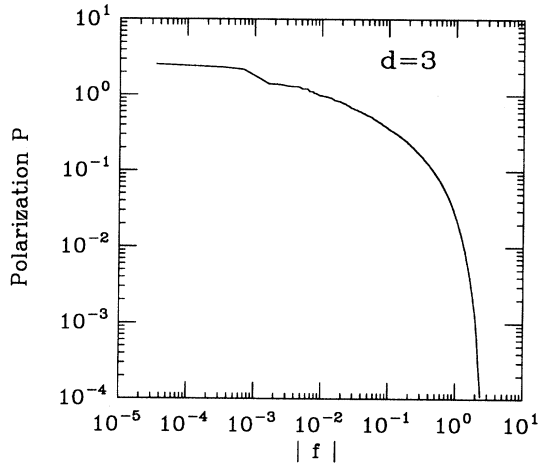

FIG. 15. Polarization of the CDW in $d=3$, for a system for size 45^3.

vs "marginal" stability. Due to the nature of the coupling between nearest neighbors in the model, all avalanches in $d=1$ at threshold are as large as the system size. The system builds up to the point where all but one site has a curvature which is within 1 of the threshold curvature C_T. Hence the hopping of any site causes a cascade which triggers the entire system into hopping, and a distribution of avalanche sizes has a spike at the system size L. This is a state of "minimal stability." In higher dimensions, the minimally stable state operative in $d=1$ is, in fact, unstable because of the extra connectivity inherent in higher dimensions. (The so-called "limited local" sandpiles[9] implement extra connectivity in $d=1$ through more extended interactions to generate nontrivial avalanche statistics.) As a result, the distribution of avalanche sizes is nontrivial, exhibiting a rough power-law falloff. This is a state of "marginal stability."

We introduced the distribution of avalanche sizes $D(s)$ to define a correlation length below threshold. At threshold, the rate of falloff of $D(s)$ is of interest. We plot, in Fig. 16, $D(s)$ for large systems in $d=2$ and 3. (The distribution is trivial in $d=1$ because of the minimal stability of the CDW.) We define an avalanche size exponent α_1 via the relation

$$D(s)\sim s^{-\alpha_1}, \quad (f=0) , \tag{50}$$

for $D(s)$ measured at threshold. From the data presented here, we estimate

$$\alpha_1=\begin{cases}1.0\pm0.05, & d=2 ,\\ 1.4\pm0.1, & d=3 .\end{cases} \tag{51}$$

We also consider the distribution of avalanche times $D(t)$ and define an exponent for its falloff:

$$D(t)\sim t^{-\alpha_2} \quad (f=0) . \tag{52}$$

Again, from fitting simulation data, which we present in Fig. 17, we find

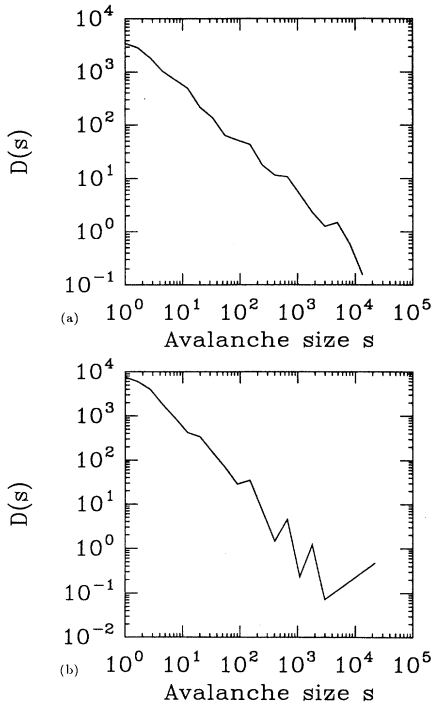

FIG. 16. Distribution of avalanche sizes $D(s)$ at threshold, in $d=2$ and 3, demonstrating a rough power-law falloff in spatial correlations. Extracted from the falloff is the exponent α_1. We find $\alpha_1=0.99$ in $d=2$ and 1.35 in $d=3$.

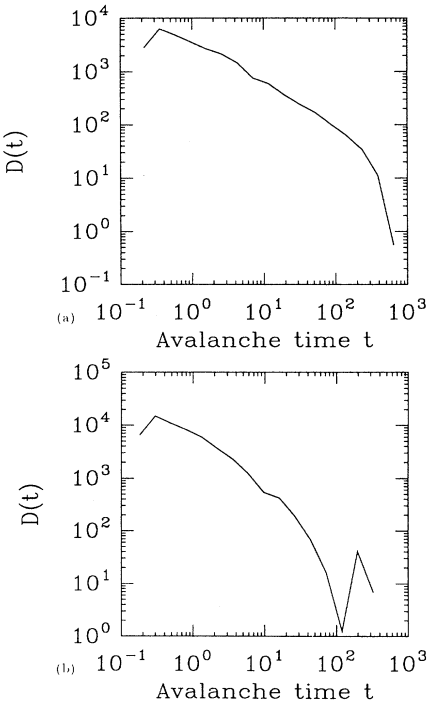

FIG. 17. Distribution of avalanche time $D(t)$ at threshold, in $d=2$ and 3, demonstrating a power-law falloff in temporal correlations. Extracted from the falloff is the exponent α_2. We find $\alpha_2=0.80$ in $d=2$ and 1.1 in $d=3$.

$$\alpha_2 = \begin{cases} 0.8 \pm 0.1, & d=2 \ , \\ 1.1 \pm 0.2, & d=3 \ . \end{cases} \tag{53}$$

Tang and Bak[26] have measured these exponents in the Bak-Tang-Wiesenfeld (BTW) sandpile model;[8] transcribed to our notation, they find that $\alpha_1 = 1.0$, 1.33 and $\alpha_2 = 0.4, 0.9$ in $d = 2, 3$, respectively. In other words, α_1 is the same for the BTW sandpile and our time-lag automaton, but α_2 is not. It appears that the spatial characteristics of the threshold configuration in our automaton CDW are equal to those of the BTW sandpile at the self-organized critical point, but the existence of the time-lag alters the temporal characteristics. This is intriguing since the scaling of the dominant time scale above threshold, namely, the CDW period T, appears to be unaffected by the existence of the time lag.

In addition to probing the threshold state by driving it from equilibrium to study avalanches, we can probe its static character in the absence of any driving other than the applied field F_T. We are particularly interested in the distribution of curvatures $D(c)$ at threshold. In the language of our automaton model, an increase in the field F serves to "excite" more phases into a state of "activity," and the distribution of curvatures serves as an important link between the stimulus of an applied field and the response of hopping.

For a system with periodic boundary conditions, it immediately follows from the definition of the lattice Laplacian that the total net curvature in the lattice for all times is zero: $\sum_i c_i = 0$. We can imagine building up the CDW from an initially flat state to that at threshold. In the flat configuration ($n_i = 0 \forall i$), $\Delta_i^2(\phi) = \Delta_i^2(\beta) \forall i$. Since β_i are drawn uniformly from the interval [0,1), the distribution of $\Delta_i^2(\beta)$ can be calculated: it is bounded on $[-2d, +2d]$, peaked at 0, and continuous in piecewise polynomial segments of order $d+1$. For a specified field, all those phases with local curvatures c_i which exceed the activation curvature C will become active and unstable, and eventually (for $F < F_T$), the CDW will stop in a stable configuration, with $c_i \leq C \forall i$. At threshold, $D(c)$ will be bounded above by the threshold curvature C_T.

Empirically, we find that in all dimensions studied, the distribution $D(c)$ appears to be a piecewise constant function. We demonstrate this in Fig. 18, where we show $D(c)$ for large systems in $d = 2$ and 3. This differs considerably from the analogous distribution measured at threshold in the original lattice FLR model, where there appears to be a divergence in the density of curvatures at threshold.[28] This divergent distribution reflects the extra strain accumulated near threshold which renders the threshold state unique in the lattice FLR model.

C. The critical dynamics of the sliding state

The bifurcation of the last fixed point at threshold signals the onset of the sliding state. Within this class of models, for $F > F_T$, the CDW converges to a steady-state periodic orbit[4] of period T, such that the average velocity v is given by $v \equiv 1/T$. The behavior of v with the reduced field f is quite complicated, as is shown in Fig. 19, a log-log plot of the velocity as a function of the reduced driving field for (a) a single two-dimensional sample of size 256^2, and (b) several two-dimensional samples of size 256^2. We distinguish four velocity regimes in finite-size systems, which we have demarcated in Fig. 19(a). Region I is the single-particle finite-size regime, where all phases hop as part of a single sliding domain, dominated by the critical site at threshold. Region II is the few-particle sparse finite-size regime, where there is more than one sliding domain participating in the motion. Region III is the critical regime, where the system obeys power-law scaling characteristic of an infinite-sized CDW and involves the simultaneous motion of many velocity-correlated domains. And region IV is the high-field crossover regime, a nonscaling regime which asymptotically approaches linear scaling at infinite f. Regions I and II together comprise the finite-size regime in this system, which we describe in more detail in the following paper. We note here, however, that the critical regime (region III) is quite small, even in a system as large as 256^2. This is due in part to the fact that the finite-size regime is so prominent in this system, such that finite-size effects become apparent when the velocity-velocity correlation length ξ is still rather small.

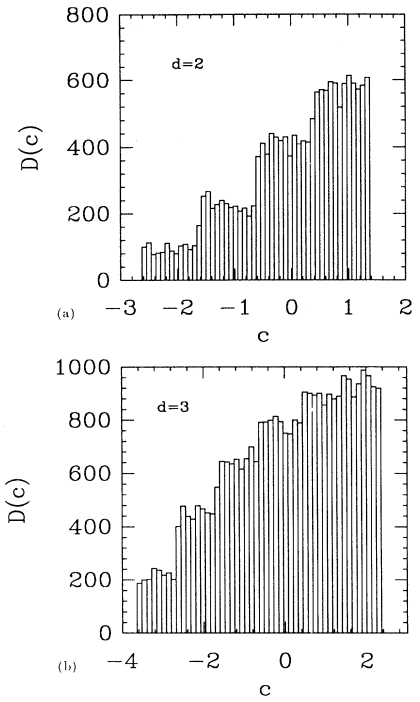

FIG. 18. Distribution of curvatures $D(c)$ in $d = 2$ and 3, for the time-lag automaton model. Each distribution is bounded above by the threshold curvature C_T. Note that $D(c)$ is basically flat for $c \lesssim C_T$.

In the critical regime, the velocity v scales as a power with reduced field f, as does the correlation length ξ. The scaling exponents ζ and ν can be related by the dynamic exponent z, which describes the time t required for a region of linear size l to hop: $t \sim l^z$. This then yields the relation

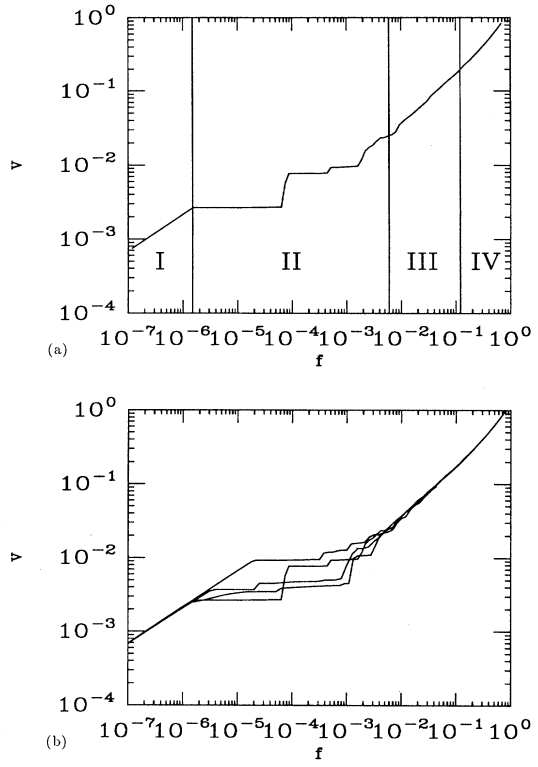

FIG. 19. CDW velocity v as a function of reduced driving field f, in (a) a single two-dimensional sample of size 256^2 and (b) several two-dimensional samples of size 256^2. Region III is the critical scaling regime where $v \sim f^{\zeta}$.

$$\zeta = z\nu \ . \tag{54}$$

In the standard formalism of dynamic critical phenomena, ν and z are the fundamental exponents, with ζ being a derived exponent. Within the context of CDW's, however, ζ has assumed a primary importance because of its direct relevance to experimental I-V measurements.

The dynamic correlation in the sliding state can be probed in a manner which is reminiscent of the study of avalanches below threshold. Each phase hops at a specific time in the periodic cycle; the spatial variation of these times gives insight into the structure and correlation of local "sliding domains" (akin to the well-defined avalanches below threshold). We can demonstrate this dynamic correlation graphically by shading each site on the lattice by a grayscale appropriate for its hopping time, for a particular sample at a fixed value of f. In Fig. 20, we do so at two different values of f: Fig. 20(a) shows a two-dimensional sample of size 128^2 at a reduced field of $f=0.01$, and Fig. 20(b) shows the same system at a field $f=0.005$, when the system is near the onset of the finite-size regime. We identify the velocity-velocity correlation length ξ above threshold as the typical linear extent of these sliding domains, although we can estimate it more precisely by examining a correlation function of the hopping times, as is done below.

As f is increased through the critical regime, the linear extent of each sliding domain ξ decreases as $\xi \sim f^{-\nu}$, and the time T for each of the domains to simultaneously hop through a full wavelength diminishes as $T \sim f^{-\zeta}$. Since the domain size diminishes as f increases, the total number of domains increases with f, as new sites become independently unstable (without having to be destabilized by an avalanche nearby). In the finite-size regime, the introduction of new sliding domains leads to abrupt jumps in the velocity since there are relatively few domains present. In the critical regime, however, the number of domains is sufficiently large that (in the thermodynamic limit) the dependence of v on f is smooth.

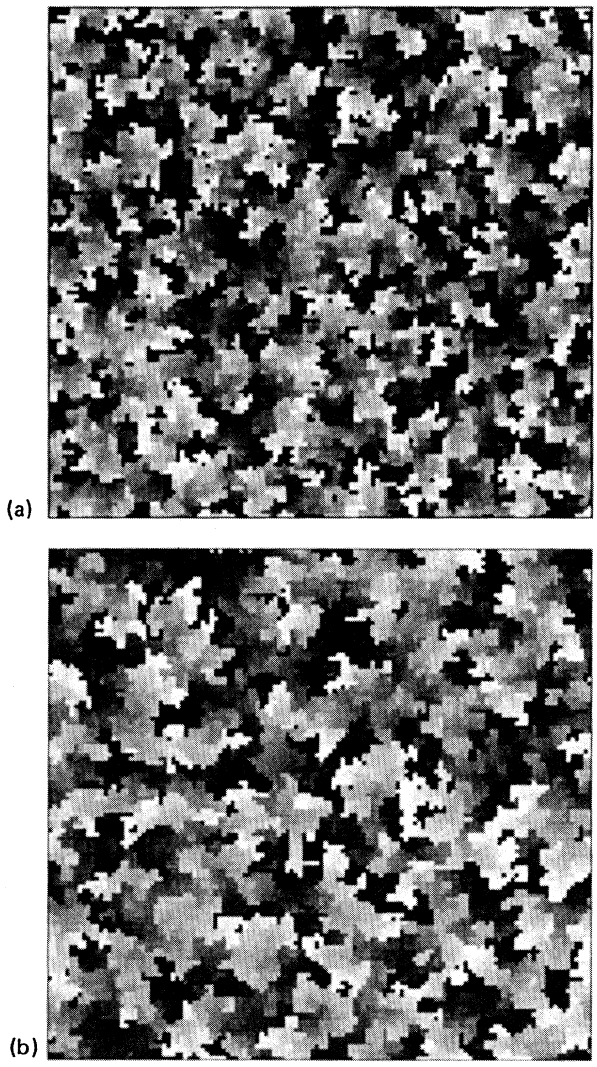

FIG. 20. Grayscale shading plot of the hopping times in a system of size 128^2 at two different values of the reduced field f. Each site is shaded according to its hopping time in the periodic orbit achieved at a fixed f: early to late times proceed from black to white, with the orbit arbitrarily initialized at the hopping of the threshold site. The average size of local hopping avalanches, or sliding domains, is the velocity-velocity correlation length ξ. In (a) $f=0.01$ and in (b) $f=0.005$; note that ξ is slightly larger at the lower field in (b).

D. Estimates of ζ

The advent of a scaling theory for the depinning transition has made the determination of the numerical value of the velocity exponent ζ (in various dimensions d) a primary task. The single-coordinate model yields a velocity exponent $\zeta_0=\frac{1}{2}$, but there is no diverging correlation length in the model since it has only one spatial degree of freedom. The emphasis of much work on FLR-type models is that nontrivial critical behavior arises from the collective dynamics of many interacting degrees of freedom. The mean-field result of $\zeta_{\rm MFT}=\frac{3}{2}$ (for a sufficiently smooth, e.g., sinusoidal, pinning potential[7]) and the expectation that FLR-type models in finite dimensions would show $\zeta\neq\frac{1}{2}$ has suggested the possibility of experimentally confirming the many-degree-freedom character of sliding CDW's by measuring an exponent different than $\frac{1}{2}$.

Accurate numerical determination of ζ in finite dimensions is quite difficult, however, because of the prominent finite-size regime at low fields and the slow nonscaling crossover at high fields. Middleton[4] has pointed out that because the crossover at high fields is so gradual, one can be misled by a simple straight-line fit on a log-log plot of the velocity.[29] More useful in determining the extent of the critical regime and estimating the exponent ζ is a determination of the local slope on a log-log plot of the velocity, which we define as

$$\zeta_{\rm loc}\equiv\frac{d(\log_{10}v)}{d(\log_{10}f)} . \tag{55}$$

Only in those intervals where this local exponent is constant does the velocity exhibit true power-law scaling. In the high-field crossover region, $\zeta_{\rm loc}$ gradually drifts upward.

Before presenting results for ζ, we decompose the period T in a manner which provides insight into the scaling behavior of v. We write T as the product of the inverse of the time-averaged density of active sites $\langle n_{\rm ac}\rangle^{-1}$ and the spatially-averaged active time $\bar{\tau}$:[30]

$$T\equiv\bar{\tau}\langle n_{\rm ac}\rangle^{-1} , \tag{56}$$

where

$$\langle n_{\rm ac}\rangle\equiv\frac{1}{T}\int_0^T dt\, n_{\rm ac}(t) \tag{57}$$

and

$$\bar{\tau}=\frac{1}{N}\sum_i \tau_i . \tag{58}$$

Alternatively, we can write

$$v\equiv\bar{\tau}^{-1}\langle n_{\rm ac}\rangle . \tag{59}$$

This decomposition is useful for several reasons. We find that $\langle n_{\rm ac}\rangle$ scales as a power law with reduced field over a considerably larger range than does the velocity. In particular,

$$\langle n_{\rm ac}\rangle\sim f^{\delta} \tag{60}$$

not only in the critical regime, but also through much of the high-field crossover. We can define a local active site density exponent

$$\delta_{\rm loc}\equiv\frac{d(\log_{10}\langle n_{\rm ac}\rangle)}{d(\log_{10}f)} , \tag{61}$$

and we find that it is roughly constant over a larger range in reduced field than is the velocity exponent $\zeta_{\rm loc}$. We can also define a local exponent $\psi_{\rm loc}$ for the average active time $\bar{\tau}$:

$$\psi_{\rm loc}\equiv\frac{d(\log_{10}\bar{\tau})}{d(\log_{10}f)} . \tag{62}$$

In practice, we do not find a regime where $\psi_{\rm loc}$ is constant, i.e., where $\bar{\tau}\sim f^{\psi}$, other than for $\psi_{\rm loc}=0$.

As mentioned before, the high-field deviations from the critical regime are associated with an upward drift in the local velocity exponent $\zeta_{\rm loc}$. The source of this upward drift appears to come entirely from the behavior of $\bar{\tau}$, the mean of the distribution of active times $D(\tau)$. To demonstrate this, we plot in Fig. 21 the velocity v, the density of active sites $\langle n_{\rm ac}\rangle$, and the average active time $\bar{\tau}$ for a system of size 256^2 [that shown in Fig. 19(a)] and the associated local exponents $\zeta_{\rm loc}$, $\delta_{\rm loc}$, and $\psi_{\rm loc}$.

We can understand the variation of $\bar{\tau}$ and f if we consider the distribution of active times $D(\tau)$, where τ_i is the amount of time that site i remains active, from when it is first activated in the periodic cycle to when it finally hops. We plot, in Fig. 22, $D(\tau)$ for various fields f. $D(\tau)$ has a long-time tail that decays as $\tau^{-3\pm0.005}$, which we argue arises from the square-root scaling of τ with excess local curvature $\Delta c_i\equiv c_i-C$ and the flat distribution of curvatures at threshold (described in Sec. III B). We can write the distribution of active times $D(\tau)$ as a function of the distribution of excess curvatures $D(\Delta c)$, via

$$D(\tau)\sim\int d(\Delta c)D(\Delta c)\delta[\tau-(\Delta c)^{-1/2}] , \tag{63}$$

where the δ function $\delta[\tau-(\Delta c)^{-1/2}]$ specifies the inverse square-root scaling of τ_i with Δc_i. Since we find empirically a flat distribution of curvatures near threshold, it follows that

$$\begin{aligned} D(\tau)&\sim\int d(\Delta c)\delta[\tau-(\Delta c)^{-1/2}] \\ &\sim\int d(\Delta c)\delta(\Delta c-\tau^{-1})(\Delta c)^{3/2} \\ &\sim(\Delta c)^{3/2}\big|_{\Delta c=\tau^{-2}} \\ &\sim\tau^{-3} . \end{aligned} \tag{64}$$

The tail of this distribution is cut off, however, by the period T, since no site can remain active for a time longer than the full period T. As T increases with decreasing f, the cutoff in $D(\tau)$ moves out further into the tail, and the mean $\bar{\tau}$ saturates with further decreases in f since the contribution to the mean from the tail becomes vanishingly small. Therefore, as f is lowered from the high-field crossover regime, $\bar{\tau}$ saturates to a constant value and $\zeta_{\rm loc}$ becomes constant, signaling the onset of power-law scaling in the critical regime. The rather rapid falloff of this

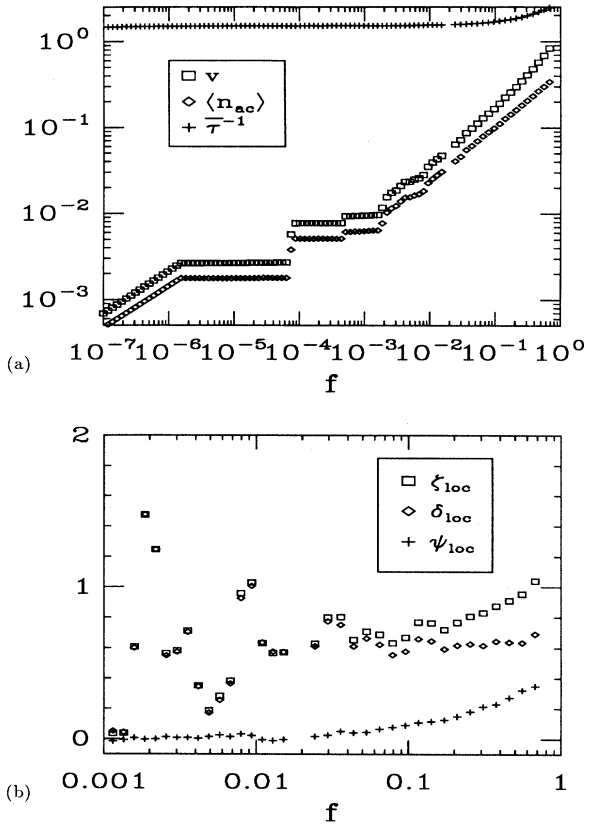

FIG. 21. The velocity v, average density of active sites $\langle n_{ac} \rangle$, and the inverse average active time $\bar{\tau}^{-1}$ as a function of f for a single sample of size 256^2 (a), and associated local exponents ζ_{loc}, δ_{loc}, and ψ_{loc} (b). ζ_{loc} is constant only over a small interval in f, once ψ_{loc} flattens out to zero. The active site density exponent δ_{loc} is seen to be roughly constant well into the high-field crossover regime when the velocity has ceased to scale as a power law. The drift in ζ_{loc} at large fields arises from the drift in ψ_{loc}.

distribution also provides insight into the fact that ζ is equal in automata with and without[31] time lags. If the distribution were to fall off sufficiently slowly, then it might conceivably have an effect on the scaling of the period T with f.

In any case, because $\bar{\tau}$ saturates at a nearly constant value, ζ_{loc} tends toward a constant value of

$$\zeta \approx \delta \ . \tag{65}$$

The velocity appears to grow in the same manner as the inverse density of active sites, in the critical regime. Even in very large systems, the critical regime is rather small; therefore, we can use the constancy of δ_{loc} to aid in determining ζ. In practice, we estimate ζ by attempting to measure a constant range in ζ_{loc}, and confirming that $\zeta_{loc} \approx \delta_{loc}$. In systems where we are unable to find a critical velocity regime, however, such as in higher dimensions where our linear sizes L are necessarily smaller, we can still measure δ_{loc} to get at least a rough estimate of ζ.

We now present results from simulations to estimate

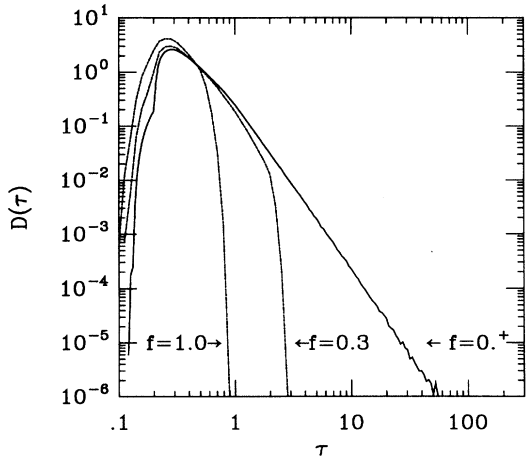

FIG. 22. Distribution of active times $D(\tau)$, for various driving fields f in $d=2$. The distributions are ensemble averages over many small systems at the specified driving fields. [We define that $D(\tau)$ is self-averaging even though the CDW velocity is not.] The cutoff in $D(\tau)$ is approximately T, which moves out to longer times at lower fields. $D(\tau) \sim \tau^{-3}$ for large τ at $f=0^+$.

the velocity exponents ζ. In Fig. 23, we show $v(f)$ for our largest samples in $d=1$ ($L=8192$) and in Fig. 24 we show the associated local exponents, ζ_{loc} and δ_{loc}. Figures 25 and 26 show velocity data and associated local exponents in two dimensions for samples of size 256^2, while the three-dimensional data is plotted in Figs. 27 and 28, for samples of size 45^3. In $d=3$, we begin to suffer from the inability to go to large enough linear system sizes L to resolve the critical regime. From these plots, we estimate that

$$\zeta = \begin{cases} 0.45 \pm 0.05, & d=1 \ , \\ 0.65 \pm 0.05, & d=2 \ , \\ 0.80 \pm 0.1, & d=3 \ . \end{cases} \tag{66}$$

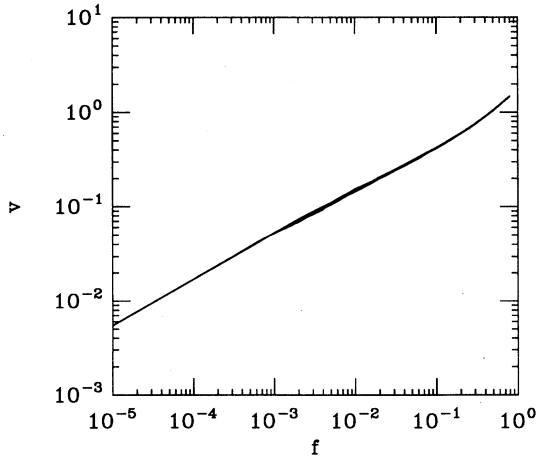

FIG. 23. CDW velocity $v(f)$ in $d=1$ for five samples of size $N=8192^1$.

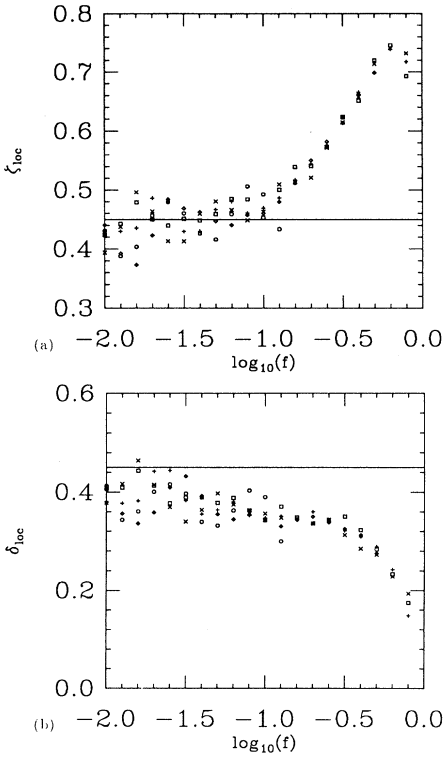

FIG. 24. Local exponents in $d=1$, for the velocity data shown in Fig. 23: ζ_{loc} in (a), and δ_{loc} in (b).

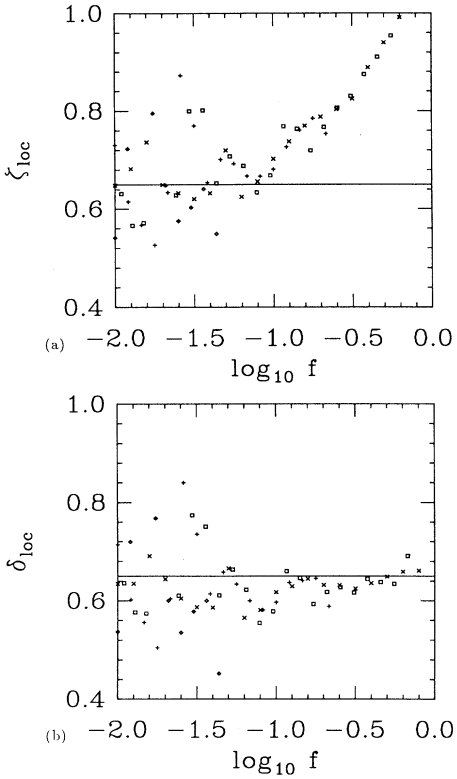

FIG. 26. Local exponents in $d=2$, for the velocity data shown in Fig. 25: ζ_{loc} in (a), and δ_{loc} in (b).

The error estimates reflect the typical fluctuations of the local exponent ζ_{loc} about the estimated ζ.

These results for ζ agree to within error for those measured by Middleton in simulations of the lattice FLR model,[4] a "racheted-kick" model,[4] and a simplified automaton model (i.e., similar to our automaton, but without the time lag).[31] Also, Narayan and Fisher's $4-\epsilon$ expansion yields, to $O(\epsilon)$, estimates of ζ equal to $\frac{1}{2}, \frac{2}{3}$, and $\frac{5}{6}$ in $d=1$, 2, and 3, respectively, which are in agreement with our results. Given the miniscule extent of the critical regime observed in simulations, the prospect of confirming these results experimentally appears difficult, as we describe in further detail in our companion paper on finite-size effects.

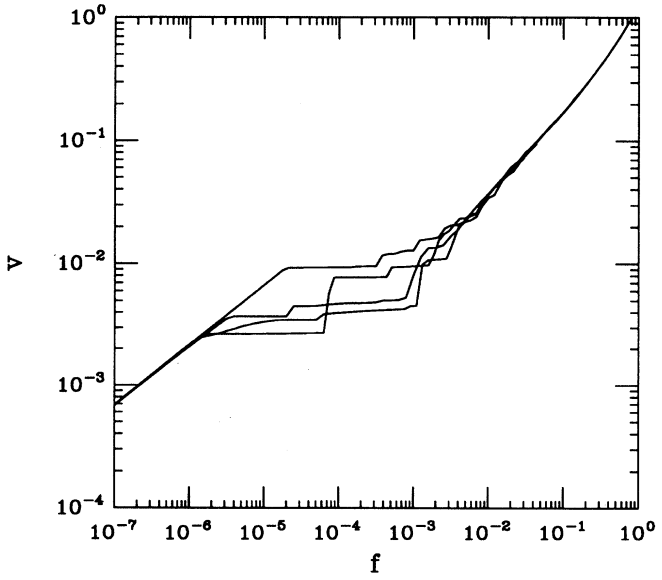

FIG. 25. CDW velocity $v(f)$ in $d=2$ for four samples of size $N=256^2$.

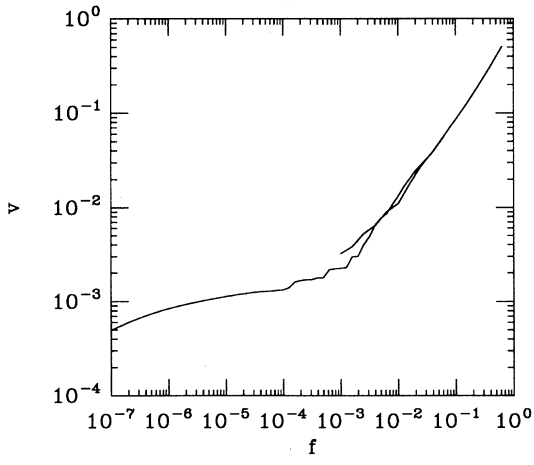

FIG. 27. CDW velocity $v(f)$ in $d=3$ for two samples of size $N=45^3$.

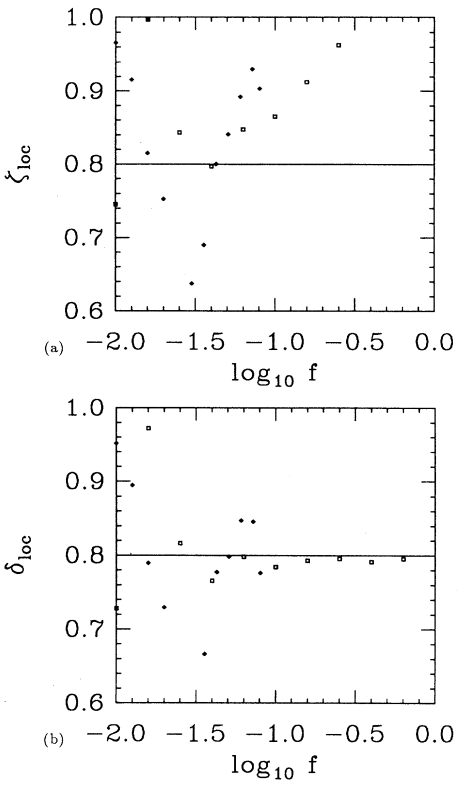

FIG. 28. Local exponents in $d=3$, for the velocity data shown in Fig. 27: ζ_{loc} in (a), and δ_{loc} in (b).

E. Estimates of ν

The exponent ν describes the critical scaling of the velocity-velocity correlation length ξ. In mean-field theory[1,7] $\nu_{MFT}=\frac{1}{2}$, a result which is uncorrected to $O(\epsilon)$ in Narayan and Fisher's $4-\epsilon$ expansion,[7] and which may be uncorrected to all orders in ϵ.[23] Previous simulations[3] have reported $\nu=0.2\pm0.1$, 0.38 ± 0.05, and 0.36 ± 0.10 in $d=1$, 2, and 3, respectively, but evidence suggests that critical scaling was not achieved in those calculations. Compared with studies of the exponent ζ, rather little effort has been directed toward measuring ν, in part because of the considerable computational burden associated with the evaluation of velocity-velocity correlation functions.

A velocity correlation length of ξ does not imply that all phases within a volume ξ^d have identical velocities $\dot{\phi}_i(t)$ for all t. Nor does it suggest that regions separated by distances larger than ξ move with different *average* velocities v, since in the absence of phase slip all regions move with the same average velocity. Rather, ξ describes the size of regions which slide as part of a local avalanche. On length scales substantially larger than ξ, many local avalanches slide simultaneously and collide with one another. This should be clear from the graphical representation of the dynamics introduced earlier in this section.

We define a velocity-velocity correlation function $C(r,t)$:

$$C(r,t)=\langle \dot{\phi}(r',t')\dot{\phi}(r'+r,t'+t)\rangle \ . \tag{67}$$

The velocities $\dot{\phi}_i(t)$ of individual phases are highly nonuniform in time, and in our automaton model they are formally treated as δ-functions in time:

$$\dot{\phi}(r_i,t)=\delta(t-t_i) \ , \tag{68}$$

where t_i is the hopping time of site i. Using (68), $C(r,t)$ becomes

$$C(r,t)=\langle \delta(t'-t_i)\delta(t'-t_j)\rangle \ , \tag{69}$$

where $r=|r_i-r_j|$.

This represents a correlation of the hopping times t_i. The motions of two sites are correlated if they hop at nearly the same time in the cycle. The motion of the CDW is periodic, so we need to consider the correlation of the hopping times modulo the period T. We do this by casting the hoping times t_i into so-called hopping angles θ_i, where

$$\theta_i=2\pi\frac{t_i(\mathrm{mod}T)}{T} \ . \tag{70}$$

We then treat the angles θ_i as if they were spins in a spin system, and evaluate the correlation function

$$C(r,t)=\langle \theta_i\cdot\theta_j\rangle \ . \tag{71}$$

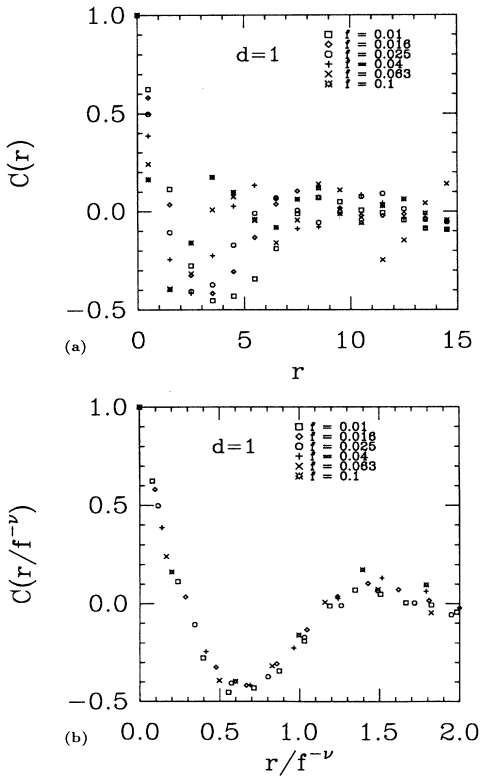

FIG. 29. Velocity-velocity correlation function $C(r)$ in $d=1$ in a single sample of size 128^1, for a range of reduced fields. (a) shows the raw correlation functions, while (b) shows scaled data to extract the correlation length exponent ν.

The angle brackets denote an average over all possible origins i. We evaluate this correlation function individually for each sample (at different values of f); we do not perform an average over the disorder.

We have computed the correlation function $C(r,t)$ in $d=1$, 2, and 3, for fields in the critical scaling regime. These results are plotted in Figs. 29–31 for $d=1$, 2, and 3, respectively; also shown are collapses of the correlation functions to extract the correlation length exponent ν. From these scalings, we estimate

$$\nu=\begin{cases}0.4\pm0.1, & d=1\ ,\\ 0.5\pm0.1, & d=2\ ,\\ 0.5\pm0.1, & d=3\ .\end{cases} \tag{72}$$

These results are consistent with the RG calculation of Narayan and Fisher,[7] and lend support for their conjecture that $\nu=\frac{1}{2}$ to all orders in ϵ. It has been noted that this correlation length exponent appears to violate the bound $\nu\geq 2/d$ which applies to (finite-size scaling) correlation length exponents in disordered systems. We address this issue in the companion paper.

The correlation functions plotted exhibit oscillations, which are most pronounced in $d=1$ and become less pronounced as d increases. These oscillations reflect the domain structure revealed in plots of the hopping times.

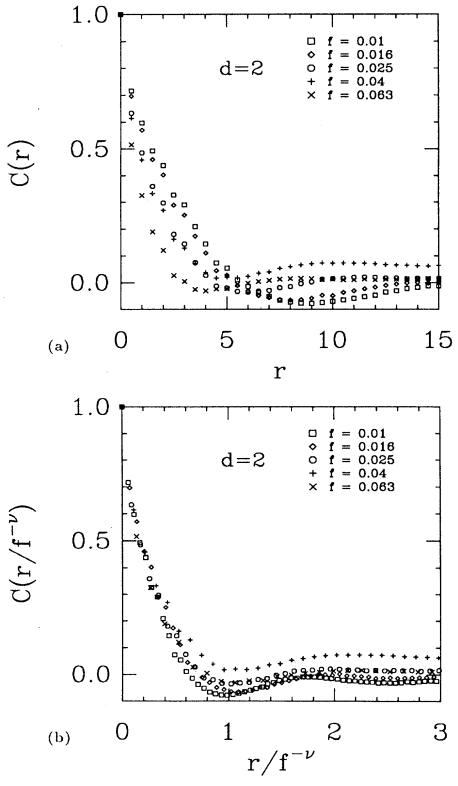

FIG. 30. Velocity-velocity correlation function $C(r)$ in $d=2$ in a single sample of size 128^2, for a range of reduced fields. (a) shows the raw correlation functions, while (b) shows scaled data.

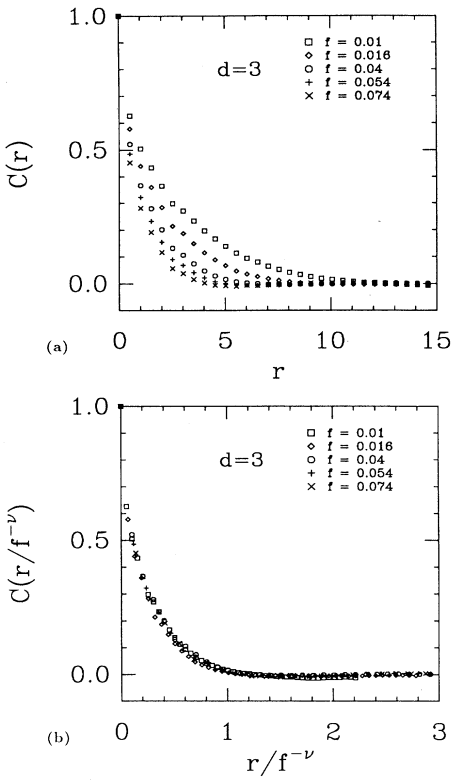

FIG. 31. Velocity-velocity correlation function $C(r)$ in $d=3$ in a single sample of size 32^3, for a range of reduced fields. (a) shows the raw correlation functions, and (b) shows scaled data.

A peak in $C(r)$ at $r=r'$ arises from having two sites a distance r' apart hopping at roughly the same time in the cycle. The strong correlation near $r=0$ reflects the local propagation of an instability, i.e., a correlated sliding domain. The peaks in $C(r)$ at larger distances, however, reflect independent, uncorrelated instabilities initiated in neighboring domains.

IV. DISCUSSION AND CONCLUSIONS

A. Automaton model and universality

Our discrete-phase time-lag automaton model was intended to treat as faithfully as possible the actual dynamics of the original lattice FLR model without having to numerically integrate through the slow motions which characterize the CDW near its sticking points. This was done with the belief that the important and relevant aspect of the CDW dynamics was the hopping of unstable phases and the subsequent destabilization of neighboring phases in an avalanche process. At the time the automaton was first constructed, little was understood with regard to the universality of the critical behavior of various models. In the last two years, in addition to our work on the time-lag automaton, Middleton has established firm numerical estimates of critical exponents in the lattice FLR model and a variety of models intended to characterize that model. The recent RG calculation of Narayan

and Fisher[7] was motivated in part by the unexpected universality which has emerged from numerical simulations on these different models, and the results of that calculation agree quite well with the established numerical results.

Despite the agreement of the exponent ζ measured in several models, the full universality of these models has yet not been explored. In particular, the correlation length exponent ν has only been measured in our automaton model (if we neglect previous simulations of the lattice FLR model which appear not to have reached the critical regime). Finite-size scaling correlation length exponents have been measured in a variety of models,[4] but it is clear that the intrinsic correlation length ξ scales in a manner different than the finite-size effects, as described in the next paper. Studies of the BTW sandpile model[26] yield values for ζ in $d=2$ and 3 essentially equal to those established in CDW models, but the reported values for ν are considerably larger than those presented here. Given the somewhat unusual nature of the universality in these systems,[7] it is clear that further work is required to establish the full extent of universality in this class of models.

In retrospect, from the point of view of computing the exponent ζ, we did not have to mimic the dynamics of the original lattice FLR model in such baroque detail. Simplified automata with[32] and without[31] time lags yield equivalent values for ζ. The existence of the time lag, and hence a second set of time scales in the problem, does, however, introduce nontrivial behavior to other aspects of the CDW dynamics, such as the finite-size regime. And the inclusion of procedures required for the "no passing" rule to be satisfied are necessary for periodic orbits to converge properly.

B. Symmetry about the transition

Critical systems typically exhibit some sort of symmetry about the critical point, most often in the equality of the exponents ν and ν' describing the divergence of the correlation length above and below the transition. From the scaling collapses presented earlier in the section, it is clear that the correlation length exponents ν and ν' are equal to within errors, in $d=2$ and 3. In $d=1$, $\nu' \gg \nu$. We feel this is most likely due to the fact that we probe correlations below threshold via avalanches, which are extremely sensitive to the minimal stability which dominates the CDW close to threshold in $d=1$. We can extract correlation lengths directly from the distributions presented earlier, and find that not only do these lengths scale in the same manner above and below threshold (for $d \geq 2$), but they appear to have the same magnitude as well. We demonstrate this in Fig. 32, for a single sample in $d=2$.

We defined a correlation time exponent ζ' below threshold in part to test whether it exhibits a symmetry with the velocity exponent ζ above threshold. Again, the statistics in $d=1$ are overwhelmed by the minimal stability of the CDW, but even for $d \geq 2$, the exponents appear not to be equal. (A case for equality could be made in $d=2$, but clearly not in $d=3$.) Even though the correlation time we defined from avalanche distributions seems

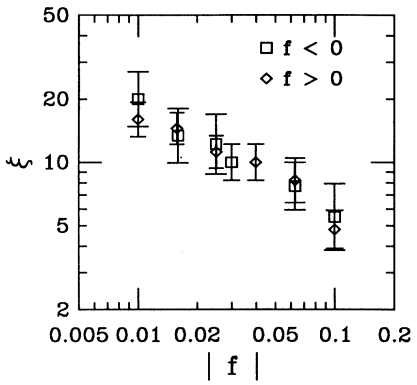

FIG. 32. A comparison of correlation lengths above and below threshold, in a two-dimensional sample of size 128^2. The lengths not only scale with roughly the same exponent, but have the same magnitude as well.

to be a natural characteristic time below threshold, it behaves differently than the characteristic time scale T above threshold. Perhaps some other time scale below threshold exists which does scale with an exponent $\zeta'=\zeta$.

Our definitions of the velocity-velocity correlation length ξ and our methods for measuring it differ considerably above and below threshold, because of the asymmetry of the order parameter about the transition. The steady-state velocity is zero below threshold, so we are forced to define ξ in a nonequilibrium fashion, i.e., by measuring the transient response of the system as it moves from one fixed point to another. Above threshold, however, the CDW slides with nonzero velocity and we are able to define an equilibrium (steady-state) correlation length based on the hopping times.

We are clearly forced to define a nonequilibrium ξ below threshold, but we are not so forced above threshold. In fact, we could define a nonequilibrium velocity correlation length describing the characteristic size of rearrangements between sliding configurations induced by a small change in driving field, or by the application of external noise to the system. We have not attempted to measure such a correlation length above threshold, but such a measurement should yield further insight into any symmetry about the critical point.

One way of symmetrically probing the system above and below threshold involves the time evolution of the density of active sites, $n_{\rm act}(t)$. In particular, we can set the reduced driving field f to a particular value and let the system relax from a "supercritical" state to a steady state suitable for that field f. We begin with the flat configuration $\phi_i=\beta_i+\frac{1}{4}$, with $n_i=0$, and monitor $n_{\rm ac}(t)$ as the CDW evolves. For $F \leq 0$ the CDW settles to a fixed point with $n_{\rm ac}(t)\equiv 0$, and for $f>0$ the CDW finds a periodic orbit with $n_{\rm ac}(t)$ periodic and nonzero for all t.

We plot $n_{\rm ac}(t)$ for a variety of driving fields f in Fig. 33. As is seen, for $f \leq 0$, $n_{\rm ac}(t)$ eventually drops to zero as the CDW becomes pinned. The time required for the pinned state to be reached, however, grows as f is increased toward zero. For $f>0$, $n_{\rm ac}(t)$ saturates at a

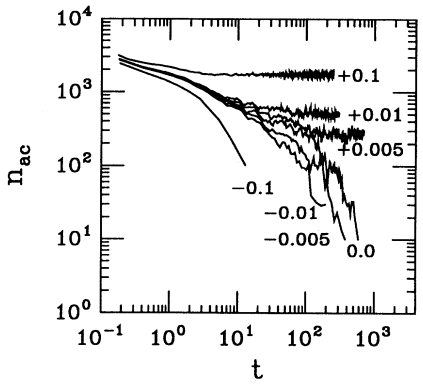

FIG. 33. The density of active sites as a function of time, $n_{ac}(t)$, for various reduced fields f. For $f \leq 0$, $n_{ac}(t)$ eventually reaches 0 at a fixed point. For $f > 0$, $n_{ac}(t)$ fluctuates about an average value as the CDW trajectory converges to a periodic orbit. The deviations from the $f = 0$ curve appear to exhibit symmetry about $f = 0$.

roughly constant nonzero value (with the time-averaged $\langle n_{ac} \rangle$ scaling like f^{δ} in the critical regime). The symmetry exhibited about threshold is revealed in the deviations of $n_{ac}(t)$ from the $f = 0$ decay. Given that the behavior of $\langle n_{ac} \rangle$ reflects the scaling of the velocity v (i.e., in the critical regime, $\zeta \approx \delta$), one could presumably symmetrically define a time scale above and below threshold from the type of information plotted in Fig. 33.

C. Summary

We have presented a study of certain aspects of the dynamics and critical phenomena of CDW's in an applied dc field. We have been particularly interested in understanding the dynamical processes which underlie the critical behavior observed in simulations. This interest has led us to define an automaton model which emphasizes the most important features of the dynamics and makes the CDW's motion simpler to characterize. The existence of at least some degree of universality among various models provides insight into some old questions while posing new ones.

TABLE I. Numerical values of the critical exponents reported here, from simulations of the discrete-phase time-lag automaton CDW's.

Expt.	Definition	$d=1$	$d=2$	$d=3$
ζ	$v \sim f^{\zeta}$	0.45±0.05	0.65±0.05	0.80±0.1
ν	$\xi \sim f^{-\nu}$	0.4±0.1	0.5±0.1	0.5±0.1
ν'	$\xi \sim (-f)^{-\nu'}$	1.1±0.1	0.6±0.1	0.45±0.1
ζ'	$t_{co} \sim (-f)^{-\zeta'}$	1.2±0.2	0.55±0.15	0.6±0.2
α_1	$D(s) \sim s^{-\alpha_1}$	NA	1.0±0.05	1.4±0.1
α_2	$D(t) \sim t^{-\alpha_2}$	NA	0.8±0.1	1.1±0.2
γ	$P \sim (-f)^{-\gamma+1}$	2.8±0.1	1.7±0.1	1.6±0.2

We have measured the velocity exponent ζ, and find it to agree with estimates obtained in simulations and analyses of a variety of other models. Furthermore, we have provided some further insight into the nature of the scaling regime by measuring the quantities $\langle n_{ac} \rangle$ and $\bar{\tau}$ and the distribution of active times $D(\tau)$. We have also measured the exponent ν describing the scaling of the correlation length ξ, and have found it to be consistent with the $4-\epsilon$ result of $\nu = 1/2 + O(\epsilon^2)$. The prominent and unusual finite-size effects seen above threshold are discussed in the following paper. As part of this summary, we have compiled in Table I our estimates of all the critical exponents presented in this paper.

ACKNOWLEDGMENTS

We would like especially to thank A. A. Middleton both for numerous valuable conversations and for sharing so many of his results with us. We thank R. E. Thorne for his ongoing help, interest, and guidance. We also would like to acknowledge useful conversations with S. N. Coppersmith, D. S. Fisher, P. B. Littlewood, O. Narayan, and S. Ramakrishna. This work was supported by NSF Grants No. DMR-8451921 and DMR-9118065, and computing facilities were provided in part by the Cornell-IBM Joint Study on Computing for Scientific Research.

*Present address: Institute for Theoretical Physics, University of California, Santa Barbara, CA 93106.

[1]D. S. Fisher, Phys. Rev. Lett. **50**, 1486 (1983); Phys. Rev. B **31**, 1396 (1985).

[2]P. B. Littlewood, in *Charge Density Waves in Solids,* edited by L. P. Gorkov and G. Grüner (Elsevier, Amsterdam, 1989).

[3]P. Sibani and P. B. Littlewood, Phys. Rev. Lett. **64**, 1305 (1990).

[4]A. A. Middleton, Ph.D. thesis, Princeton University, 1990.

[5]A. A. Middleton and D. S. Fisher, Phys. Rev. Lett. **66**, 92 (1991).

[6]S. N. Coppersmith and D. S. Fisher, Phys. Rev. A **38**, 6338 (1988).

[7]O. Narayan and D. S. Fisher, Phys. Rev. Lett. **68**, 3615 (1992); Phys. Rev. B **46**, 11 520 (1992).

[8]P. Bak, C. Tang, and K. Wiesenfeld, Phys. Rev. Lett. **59**, 381 (1987).

[9]L. P. Kadanoff, S. R. Nagel, L. Wu, and S.-M. Zhou, Phys. Rev. A **39**, 6524 (1989).

[10]J. M. Carlson, J. T. Chayes, E. R. Grannan, and G. Swindle, Phys. Rev. Lett. **65**, 2547 (1990).

[11]J. M. Carlson and J. S. Langer, Phys. Rev. Lett. **62**, 2632 (1989); J. M. Carlson, J. S. Langer, B. Shaw, and C. Tang, Phys. Rev. A **44**, 884 (1991).

[12]For an introduction to CDW's, see, e.g., G. Grüner, Rev. Mod. Phys. **60**, 1129 (1988); *Charge Density Waves in Solids,* edited by G. Hutiray and J. Sólyom (Springer-Verlag, Berlin, 1985); *Charge Density Waves in Solids,* edited by L. P. Gorkov and G. Grüner (Elsevier, Amsterdam, 1989).

[13]H. Fukuyama, J. Phys. Soc. Jpn. **41**, 513 (1976); **45**, 1474 (1978); H. Fukuyama and P. A. Lee, Phys. Rev. B **17**, 535 (1977); P. A. Lee and T. M. Rice, *ibid.* **19**, 3970 (1979).

[14]N. Teranishi and R. Kubo, J. Phys. Soc. Jpn. **47**, 720 (1979); L. Petronero and S. Strässler, Phys. Rev. B **28**, 5863 (1983); H. Matsukawa and H. Takayama, Solid State Commun. **50**, 283 (1984); P. B. Littlewood, Phys. Rev. B **33**, 6694 (1986).

[15]P. B. Littlewood, Phys. Rev. B **33**, 6694 (1986); H. Matsukawa, J. Phys. Soc. Jpn. **57**, 3463 (1988); S. N. Coppersmith and D. S. Fisher, Phys. Rev. A **38**, 6338 (1988); P. B. Littlewood and C. M. Varma, Phys. Rev. B **36**, 480 (1987); P. Sibani and P. B. Littlewood, Phys. Rev. Lett. **64**, 1305 (1990); A. A. Middleton and D. S. Fisher, *ibid.* **66**, 92 (1991); A. A. Middleton, Ph.D. thesis, Princeton University, 1990; A. A. Middleton and D. S. Fisher, Bull. Am. Phys. Soc. **36**, 766 (1991).

[16]The instability of the FLR model arising from this harmonic coupling has been discussed in S. N. Coppersmith, Phys. Rev. Lett. **65**, 1044 (1990).

[17]A. A. Middleton, Phys. Rev. Lett. **68**, 670 (1992).

[18]A different type of weak-coupling approach was pursued in S. N. Coppersmith, Phys. Rev. A **36**, 3375 (1987).

[19]The tendency of $C_T \to \frac{1}{2}$ in $d=1$ can be understood by considering the constraints imposed on the curvatures $\{c^{(n)}\}$ of the integer field $\{n\}$: $\sum_i c_i^{(n)}=0$, and $\sum_i (c_i^{(n)}-c_{i-1}^{(n)})=mN$, where m is an integer and N is the length of the periodic chain. For $d>1$, however, such constraints are more difficult to specify. Our estimates that $C_T \approx (d-1)+0.376$ for large L may be appropriate only for the system sizes we have studied. There may be further drift in C_T for larger L. The empirically determined result $C_T \approx (d-1)+0.376$ suggests that the actual behavior could be $C_T \approx (d-1)+\frac{3}{8}$, although we have no analytic result which would confirm or refute such an estimate.

[20]A. A. Middleton (private communication).

[21]We did not examine the noise spectrum of the unconverged orbits from the early version of the time-lag automaton, so we cannot speculate as to its form (e.g., $1/f^{\alpha}$).

[22]S. N. Coppersmith and P. B. Littlewood, Phys. Rev. B **36**, 311 (1987).

[23]D. S. Fisher (private communication).

[24]C. Tang, K. Wiesenfeld, P. Bak, S. N. Coppersmith, and P. B. Littlewood, Phys. Rev. Lett. **58**, 1161 (1987).

[25]A. A. Middleton (private communication).

[26]C. Tang and P. Bak, Phys. Rev. Lett. **60**, 2347 (1988).

[27]L. Pietronero and W. R. Schneider, Phys. Rev. Lett. **66**, 2336 (1991).

[28]A. A. Middleton (private communication).

[29]A. A. Middleton, in Ref. 4, points out that this is the source of the discrepancy between the values for ζ cited in his work and those cited in Ref. 3.

[30]This decomposition is exact in our automaton model, where $n_{ac}(t)$ changes by discrete amounts instantaneously.

[31]A. A. Middleton, O. Biham, P. B. Littlewood, and P. Sibani, Phys. Rev. Lett. **68**, 1586 (1992).

[32]C. R. Myers (unpublished).

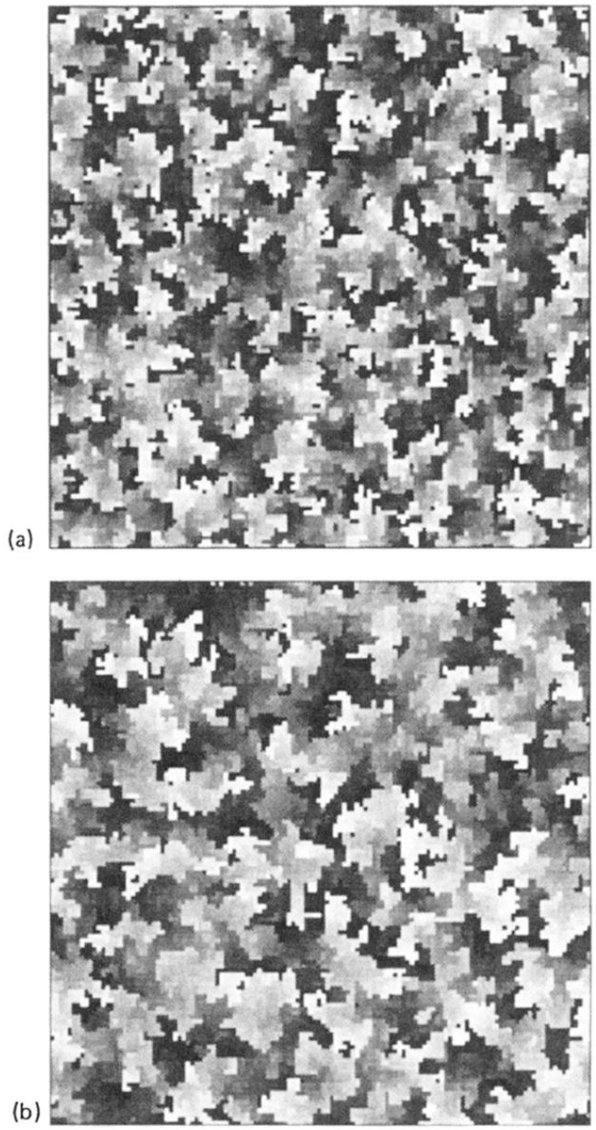

FIG. 20. Grayscale shading plot of the hopping times in a system of size 128^2 at two different values of the reduced field f. Each site is shaded according to its hopping time in the periodic orbit achieved at a fixed f: early to late times proceed from black to white, with the orbit arbitrarily initialized at the hopping of the threshold site. The average size of local hopping avalanches, or sliding domains, is the velocity-velocity correlation length ξ. In (a) $f=0.01$ and in (b) $f=0.005$; note that ξ is slightly larger at the lower field in (b).